A CASE STUDY OF RADIATIVE FORCING UPON A TROPICAL CLOUD CLUSTER

by Gregory P. Byrd
and
Stephen K. Cox

Atmospheric Science
PAPER NO.
329

US ISSN 0067-0340

DEPARTMENT OF ATMOSPHERIC SCIENCE
COLORADO STATE UNIVERSITY
FORT COLLINS, COLORADO

A CASE STUDY OF RADIATIVE FORCING UPON A TROPICAL CLOUD CLUSTER

by

Gregory P. Byrd and Stephen K. Cox

Research Supported by
The Global Atmospheric Research Program
National Science Foundation and the
GARP Atlantic Tropical Experiment (GATE) Project Office, NOAA
under grant ATM 78-05743

Department of Atmospheric Science
Colorado State University
Fort Collins, Colorado

November, 1980

Atmospheric Science Paper Number 329

ABSTRACT

Tropospheric radiative convergence profiles from Cox and Griffith (1978) are used to assess the radiative forcing upon a tropical cloud cluster located in the vicinity of the GATE A/B-scale array during 4-6 September 1974. "Slab" and cross sectional analyses are carried out in order to present a three dimensional view of the radiative convergence field within the cluster and its surrounding regions. Next, a simple vertical motion profile is constructed to investigate the potential effects of radiative forcing upon cluster scale dynamical interactions with the large scale circulation. The model is tested on a daytime and a nighttime case within the cluster life cycle. The ensuing discussion evaluates the analysis and expands upon the possible roles of radiative forcing upon cluster scale and large-scale dynamics.

Radiative forcing is strongest during the initial stages of cluster development. Throughout the cluster life cycle, the radiative forcing is consistently strongest in the middle troposphere (400-700 mb). With the intensification of the cluster system, a substantial weakening of horizontal gradients of radiative convergence occurs as a result of SW warming superimposed upon LW cooling during the daylight hours. Increased amounts of middle and high cloud remnants in regions surrounding the maturing cluster also contribute to the observed weakening of radiative forcing. The cross sectional analyses reveal that E-W gradients of radiative convergence between the cluster and its surroundings are comparable in magnitude to the N-S gradients. The maximum in cluster precipitation intensity is observed to lag the incidence of strong radiative forcing by some 6-8 hours, in general

agreement with GATE composite observations. Continental-oceanic differential heating plays a significant role in modulating the cluster and large scale dynamical interactions, accounting for the anomalously large precipitation lag observable in the GATE cluster.

The radiatively derived vertical motion model yields a qualitatively realistic total area of cluster influence for the nighttime period. The model assumption of a closed mass system breaks down during the daytime period, yielding an unreasonably large total area of influence. This suggests the occurrence of significant cluster scale interactions with large scale circulations during the daytime period. Radiative forcing appears to play a more significant role in dynamical interactions at night, when circulations appear to be somewhat more localized.

ACKNOWLEDGMENTS

The authors wish to thank Ms. Sandy Wunch, Ms. Pauline Martin and Mr. Mark Howes for their valuable assistance in the preparation of this manuscript. The research for this paper was supported by the National Science Foundation and the GATE Project Office of NOAA under grant ATM 78-05743. Computing time was furnished by the National Center for Atmospheric Research which is sponsored by the National Science Foundation.

TABLE OF CONTENTS

		PAGE
	ABSTRACT	ii
	ACKNOWLEDGEMENTS	iv
	TABLE OF CONTENTS	v
	LIST OF TABLES	vi
	LIST OF FIGURES	vii
	LIST OF SYMBOLS	x
I.	INTRODUCTION	1
II.	BACKGROUND	3
	2.1 Studies Relating to Radiative Forcing	3
	2.2 Meteorological Description of the Case Study Event.	9
III.	DATA	11
	3.1 GATE Phase III Radiative Convergence Profiles	11
	3.2 Radar Data	13
	3.3 Vertical P-Velocity Values	13
IV.	ANALYSIS	17
	4.1 Slab Analysis	17
	4.2 Cross Sections	28
	4.3 The Radiatively Derived Vertical Motion Model	41
	4.3.1 Methodology	41
	4.3.2 Results	46
	4.3.3 Model Sensitivity	54
V.	IMPLICATIONS	57
VI.	CONCLUSIONS	64
	REFERENCES	68

LIST OF TABLES

		PAGE
Table 1.	Cluster minus clear difference in total tropospheric convergence (TTC) for the cluster life cycle. Units are in Wm^{-2} $(900\ mb)^{-1}$. The differences apply over a 110 km horizontal distance and are derived from the north-south and east-west cross sections.	40
Table 2.	Profiles of various components of vertical p-velocity within the GATE A/B-scale array for 0600-1200 LST and 1800-2400 LST on 5 September 1974.	48

LIST OF FIGURES

		PAGE
Figure 1.	Comparison of typical rate of net radiation-induced temperature changes in a tropical disturbance with an opaque high cloud cover and in a tropical clear region, from information supplied by S. Cox and from other quoted radiation papers. (From Gray, 1979a).	5
Figure 2.	Hypothesized slope of pressure surfaces in the typical tropical disturbance, and the magnitude of the usual inflow (arrows). (From Gray, 1979a).	6
Figure 3.	Graphical depiction of A/B and B-scale arrays, as defined in this report. Dashed lines enclose 1/2 degree latitude by 1/2 degree longitude boxes, solid lines represent geographical latitude and longitude. Integer values centered within dashed boxes represent numbering scheme used in identifying specific areas. (From Cox and Griffith, 1978).	12
Figure 4.	Depiction of areal coverage of a) the shipboard radar shown in the photomosaics of Arkell and Hudlow (1977) during the analysis period, and b) the GATE master radar array. The solid hexagon (——) represents the A/B-scale array and the dashed hexagon (---) represents the B-scale array.	14
Figure 5.	A latitude versus longitude "slab" view of the 1800-2400 LST total (SW + LW) convergence over the A/B-scale array on 4 September 1974. The shaded area constitutes the 2230 LST radar echo area from Arkell and Hudlow (1977). The "C" denotes areas of maximum radiative cooling while the "W" denotes areas of minimum radiative cooling. Units are in Wm^{-2} 300 mb^{-1}.	18
Figure 6.	Same as Figure 5 except for 0000-0600 LST on 5 September 1974 convergence and 0430 LST radar.	19
Figure 7.	Same as Figure 5 except for 0600-1200 LST on 5 September 1974 convergence and 1030 LST radar.	20
Figure 8.	Same as Figure 5 except for 1200-1800 LST on 5 September 1974 convergence and 1630 LST radar.	21
Figure 9.	Same as Figure 5 except for 1800-2400 LST on 5 September 1974 convergence and 2230 LST radar.	22

		PAGE
Figure 10.	A pressure vs. a) latitude (at 23.5°W), and b) longitude (at 8.5°N) cross sectional view of the A/B-scale array for 1800-2400 LST on 4 September 1974. The radiative convergence units are in Wm^{-2} $(100\ mb)^{-1}$. The magnitude and direction of horizontal radiative convergence gradients are shown in areas of concentrated radiative forcing. The arrows point towards regions of smaller radiative cooling and are analogous to the hypothesized inflow-outflow regimes of Gray (1979a) shown in Figure 2.	29
Figure 11.	Same as Figure 10 except for 0000-0600 LST on 5 September 1974.	30
Figure 12.	Same as Figure 10 except for 0600-1200 LST on 5 September 1974.	31
Figure 13.	Same as Figure 10 except for 1200-1800 LST on 5 September 1974.	32
Figure 14.	Same as Figure 10 except for 1800-2400 LST on 5 September 1974.	33
Figure 15.	Conceptualization of the radiatively derived A/B-scale vertical motion model.	44
Figure 16.	Conceptualization of the radiatively derived total area (A_{TOT}).	47
Figure 17.	LW convergence and cloud top distribution for the regions surrounding the cluster for 0600-1200 LST (dashed) and 1800-2400 LST (solid) on 5 September 1974.	50
Figure 18.	Graphical depiction of the GATE cluster area (A_{up}) and the total area (A_{TOT}) for 0600-1200 LST on 5 September. The infrared satellite imagery is for 0900 LST (1030 GMT).	52
Figure 19.	Graphical depiction of the GATE cluster area (A_{up}) and the total area (A_{TOT}) for 1800-2400 LST on 5 September 1974. The infrared satellite imagery is for 2100 LST (2230 GMT).	53

PAGE

Figure 20. Sensitivity of the $\overline{\omega}_{up}$ profile to various imposed errors. A represents the model value for $\overline{\omega}_{up}$; B represents the assumption that $\overline{\omega}_{down} = 0$; C represents a 10% overestimation of cluster area; D represents a 10% underestimation of cluster area. 55

Figure 21. GATE master radar array rainfall rate (——) and the mean zonal (---) and meridional (-·-) radiative forcing from Table 1. The arrows delineate time periods when precipitation was dominated by the squall line rather than the cluster system. 59

LIST OF SYMBOLS

p	-	Pressure
T	-	Temperature
θ	-	Potential temperature
IR	-	Infrared
SW	-	Shortwave
TTC	-	Total tropospheric convergence
ITCZ	-	Intertropical convergence zone
mb	-	Millibars (1 mb = 1 dyne/cm^2)
ω	-	Vertical velocity in pressure coordinates ($\omega = dp/dH$)
g	-	Acceleration due to gravity
c_p	-	Specific heat of dry air at constant pressure
F_n	-	Net radiative flux
R	-	Gas constant for dry air
LST	-	Local standard time
GMT	-	Greenwich mean time
$\mathbb{V}$	-	Wind

I. INTRODUCTION

A primary motivation for the GARP Atlantic Tropical Experiment (GATE) was the collection of data to obtain a more thorough appreciation of cluster scale interactions with the large scale circulation. Recent studies by Albrecht and Cox (1975), Gray and Jacobson (1977) and Webster and Stephens (1980) have suggested that radiative forcing may play a significant role in these dynamical interactions. An intensive examination of the atmospheric response to gradients in radiative energy convergence is essential for a complete understanding of the role of radiation in cluster scale and large scale circulations. The radiation subprogram of GATE provided a large data base with which to carry out such an investigation. Cox and Griffith (1978), Zaitseva (1976) and Zaitseva and Fimpel (1976) have done extensive radiation budget studies utilizing GATE data.

The present study utilizes GATE total (shortwave plus longwave) radiative convergence profiles from Cox and Griffith (1978). Positive values of radiative convergence are indicative of warming and negative values denote cooling within an individual layer.

The cloud cluster in question is a relatively slow moving disturbance contained primarily within the GATE A/B-scale array during its lifetime from 1800 LST 4 September to 0000 LST 6 September 1974. The non-radiative characteristics of this cluster have been extensively analyzed by Leary and Houze (1979a,b) and Leary (1979).

The primary objective of this study is to investigate the atmospheric response to variations in radiative forcing throughout the lifetime of the cloud cluster. Since day-night variations in the radiative

convergences are superimposed upon cluster lifetime variations, special emphasis is placed upon diurnal variations as well.

A background discussion summarizes some of the previous investigations which served as motivation for the present study. The atmospheric response to gradients in radiative convergence between the cluster and its surrounding environment is examined by means of cross section and "slab" analyses over the Cox/Griffith array. A radiatively derived vertical motion model is constructed in order to obtain an estimate of the role of radiation in larger scale dynamics. A qualitative discussion provides inferences as to the significance of radiative forcing upon cluster scale as well as large scale dynamical interactions. The interpretations presented herein are based solely upon this single case study and may not necessarily be representative of cluster disturbances as a whole.

II. BACKGROUND

The three primary diabatic heating inputs into the atmosphere are latent, sensible and radiative heating. In the past, release of latent heat by convection was regarded as the primary diabatic influence in organized tropical oceanic disturbances. As a consequence, the role of convective heating has been rather extensively analyzed. Sensible and radiative heating effects were thought of as small and received only secondary consideration. Only recently have studies suggested that radiative forcing between a radiatively active cloud area and its surroundings may be of significance in modulating convection within a disturbance region. A survey of several of these investigations follows.

2.1 Studies Relating to Radiative Forcing

Albrecht and Cox (1975) have studied large scale atmospheric response to infrared heating due to variations in middle and high cloudiness. Through the use of a diagnostic model they were able to show that easterly wave structure was quite sensitive to phase modulations between convective and radiative heating. Meridional wind perturbations and mass divergence at 200 mb were much larger when the radiatively active cloud area was located one-half wavelength from the center of convective heating. When the radiatively active cloud area was centered over the convective heating, a larger convergence was observed in the lower layers, although the inflow layer was not as deep. This suggests that a radiatively active cloud area acts as a modulator of atmospheric process, regardless of whether or not the particular cloud area is associated with a region of active convection. Model results of Albrecht and Cox (1975) and of Stephens and Webster

(1979) indicate that longitudinal variations of radiative forcing are significant enough to warrant inclusion in general circulations models. Gray and Jacobson (1977) and Foltz (1976) present observational evidence indicating that, over mid-oceanic areas, occurrences of deep convection and associated heavy rain events are 2-3 times more frequent in the morning than in the late afternoon. The diurnal variation in deep convection is hypothesized to result from day versus night radiational cooling rate differences between the disturbance and the adjacent "cloud free" environment.

Figure 1 shows the radiative cooling profiles in a convective area and in a cloud free area. In a region of deep convection the higher clouds prevent longwave (LW) energy losses from lower tropospheric levels. This results in a lower LW cooling rate at low and middle tropospheric levels within the disturbance area. However, at upper levels the large LW energy losses from the cloud top region lead to significantly larger LW cooling rates in the upper troposphere. Overall tropospheric IR cooling rates are larger over cloud free regions than over disturbance regions. During the daytime, shortwave (SW) absorption tends to counterbalance LW losses, resulting in a substantial weakening of the total (SW + LW) radiative convergence gradients between the disturbance and adjacent cloud free regions. Figure 2, from Gray and Jacobson (1977) shows the hypothesized perturbation of pressure surfaces and the radial wind regime resulting from this diurnal cycle in radiative forcing. It is suggested that this radiational forcing between the disturbance and the surrounding regions is maximized at around sunrise. The atmospheric response is

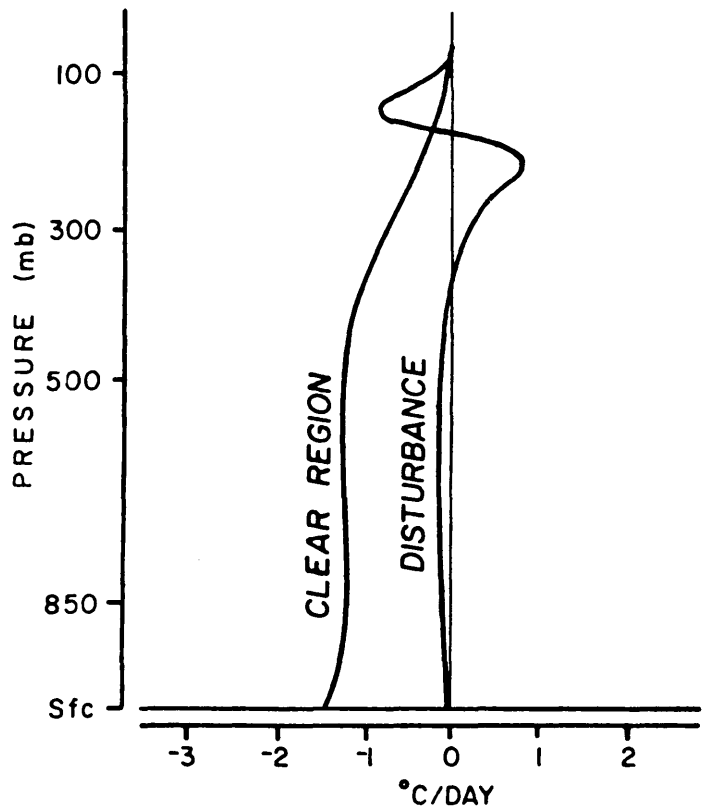

Figure 1. Comparison of typical rate of net radiation-induced temperature changes in a tropical disturbance with an opaque high cloud cover and in a tropical clear region, from information supplied by S. Cox and from other quoted radiation papers. (From Gray, 1979a).

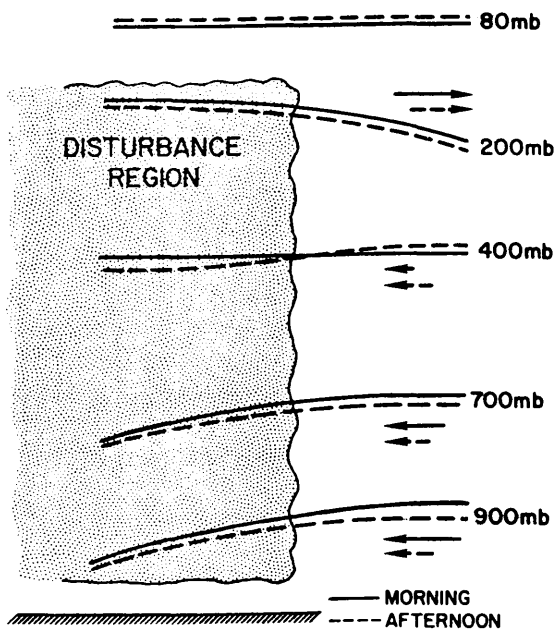

Figure 2. Hypothesized slope of pressure surfaces in the typical tropical disturbance, and the magnitude of the usual inflow (arrows). (From Gray, 1979a).

hypothesized to lag the forcing by several hours, resulting in a morning maximum in heavy precipitation events.

GATE observations did not show a morning rainfall maximum, but rather tended toward an afternoon peak. Gray and Jacobson (1977) attribute this to the stronger low level wind shear and the instances of squall line activity within the GATE area. It is worth noting that this diurnal radiative forcing argument is most applicable to mid-oceanic regions and to organized weather systems and associated heavy rainfall occurrences. Gray and Jacobson (1977) suggest that frictional convergence in the boundary layer cannot completely account for the deep inflow regions observed in tropical cloud clusters. Therefore, radiative forcing must be considered as a contributing factor to the dynamics of cloud cluster systems.

An extensive radiative convergence budget study was carried out by Cox and Griffith (1978) for Phase III of the GATE A/B-scale array. Phase III radiative convergence profiles were generally shown to have less upper tropospheric convergence and more middle level convergence than previous climatological estimates (Dopplick, 1972; Katayama, 1966, 1967a,b). A relative minimum in tropospheric radiative convergence was found in the 900-1000 mb layer for GATE Phase III profiles. The differences were attributed to the large amounts of middle and upper level cloudiness and high precipitable water during Phase III of GATE. In addition the water vapor pressure broadened continuum had not been taken into account in previous studies. The suppressed radiative cooling in the 900-1000 mb layer was in part, a consequence of the assignment of convective cloud base to the layer.

Several diurnal effects were noted in the Cox/Griffith study. Day-night variations in satellite derived cloud top distributions were found. A peak in total cloud amount and high cloudiness was observable in the 1200-1800 LST period. This tendency was most noticeable in a composite of convectively disturbed occurrences. Diurnal variations of horizontal radiative convergence gradients between a disturbed area and its surroundings seemed to account in part for the observed diurnal precipitation and cloud cover variability shown in previous investigations.

Finally, Ackerman and Cox (1980) generated radiative convergence profiles for an easterly wave composite over a broad area of the eastern Atlantic for Phase III of GATE. The composited easterly wave cloud top coverage showed greater areal cloud cover and middle and upper cloudiness during the nighttime 12 hour period. Only in the region of maximum convection was a daytime high cloud maximum observed. Zonal differences of radiative convergences at specific levels were noted. As in previous studies, the horizontal gradients in radiative convergence were larger at night. The investigation offers three possible mechanisms for the observed diurnal variability in mass convergence. These are: 1) differences in radiative convergences between the ITCZ and adjacent areas; 2) differences in radiative convergences between cluster and cloud free areas as proposed by Gray and Jacobson (1977); and 3) a nocturnal peak in radiative cooling in the upper troposphere located one-half a wavelength from the center of convective activity (Albrecht and Cox, 1975).

2.2 Meteorological Description of the Case Study Event

Some of the non-radiative properties of the 4-6 September 1974 cloud cluster have been extensively analyzed by Leary and Houze (1979 a,b) and Leary (1979). The disturbance was embedded in relatively weak flow at middle levels, resulting in anomalously slow westward propagation of 3-4 ms^{-1}. This made for an ideal case study, since the cluster was contained primarily within the A/B array during its entire life cycle.

Leary and Houze (1979a) discuss the evolution of convection within the cloud cluster, dividing the disturbance life cycle into four distinct stages. The formative period is characterized by isolated convective elements which tend to align themselves perpendicular to the mean low level flow field. This is followed by the intensification stage in which convergence is enhanced due to cell downdraft mergers, resulting in consolidation of precipitation areas. The mature stage shows heavier convective precipitation at the leading edge along with a broad, uniform area of lighter precipitation behind. Leary and Houze (1979b) offer a detailed description of mesoscale uplift occurring in middle and upper troposphere layers in association with this uniform precipitation area.

Leary (1979) examines the behavior of the wind field in response to the convective cluster. The disturbance region of 4-6 September is characterized by trade wind convergence in the lower levels, a large scale easterly wave disturbance at middle levels, and a divergent region in the easterlies at upper levels. The first notable feature during cluster formation and intensification is the initiation of a closed cyclonic wind circulation at the surface. After several hours,

a 700 mb closed cyclonic circulation develops, coincident with increased anticyclonic circulation at 200 mb. These middle and upper level wind perturbations occur despite the fact that the cluster is already in its dissipating stages. The observations seem in agreement with previous GATE studies, indicating that differing types of disturbances have qualitatively similar feedback with the large scale environment.

III. DATA

Several data sources were utilized during the present investigation. They include radiative convergence profiles for the A/B array of GATE Phase III from Cox and Griffith (1978), radar data from Arkell and Hudlow (1977) and Hudlow and Patterson (1979) and a time series of A/B array vertical motion from Nitta (1977). A brief description of each is contained in the following sections.

3.1 GATE Phase III Radiative Convergence Profiles

Cox and Griffith (1978) constructed radiative convergence profiles for 225 1/2° latitude by 1/2° longitude boxes encompassing the GATE A/B array. The 225 box array and its corresponding A/B- and B-scale regions are depicted in Figure 3. The vertical resolution for the convergence profiles consists of nine 100 mb layers and a 12 mb surface layer in the region between 1000-1012 mb. The present study utilizes five 6 hour means of radiative convergence which comprise the period 1800 LST 4 September to 0000 LST 6 September 1974.

Visible and infrared (IR) GATE SMS-1 satellite brightness data (Smith and Vonder Haar, 1976; Polifka and Cox, 1977) were used to construct cloud top distributions for the A/B array of GATE. Several corrections were applied to these data. The first involves an adjustment at levels below 500 mb for the spectral emission of water vapor in the range of the 11 μm sensor. The second accounts for distance of penetration into a cloud before realization of radiative "blackness". In addition, a sun glint correction was applied during the determination of the cloud-free area.

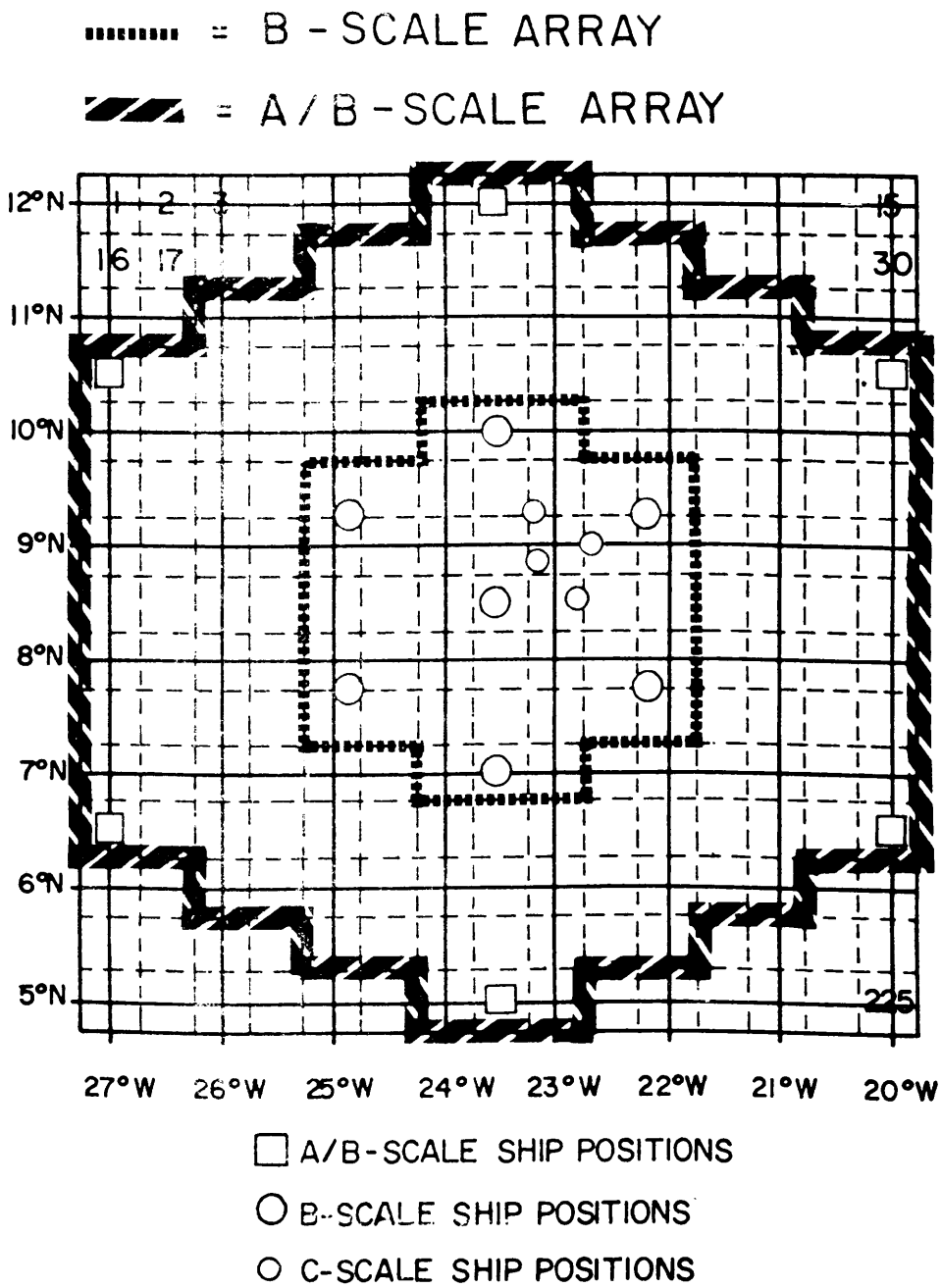

Figure 3. Graphical depiction of A/B- and B-scale arrays, as defined in this report. Dashed lines enclose 1/2 degree latitude by 1/2 degree longitude boxes, solid lines represent geographical latitude and longitude. Integer values centered within dashed boxes represent numbering scheme used in identifying specific areas. (From Cox and Griffith, 1978).

On the basis of the satellite-derived cloud information and associated synoptic data, 28 shortwave (SW) and 25 longwave (LW) convergence profiles were constructed. These profiles were in turn used in the generation of SW, LW and total (SW + LW) radiative convergence profiles over the 225 box array. Cox, et al. (1976) describe the integral absorptance model used in the calculation of the SW convergence profiles. An in-depth description of the integral emittance LW radiative transfer routine employed in the calculation of the LW divergence profiles is contained in a paper by Cox (1973). Both models underwent adjustments to take into account radiation observations in GATE. For a more detailed account of the methodology involved in the determination of the vertical profiles of radiative convergence, the reader is referred to Cox and Griffith (1978; 1979a,b).

3.2 Radar Data

Arkell and Hudlow (1977) constructed photomosaics of radar data from the GATE ships Gillis, Quadra, Oceanographer and Researcher which are superimposed upon the "slab" analyses of radiative convergence in the present study. These photomosaics covered a major portion of the A/B array during Phase III of GATE. Radar-derived rainfall rates from Hudlow and Patterson (1979) for a 200 km circle encompassing the B-scale array are included in a later discussion. The coverage areas for each of the radar sets and their relationships to the GATE arrays are depicted in Figure 4a,b.

3.3 Vertical P-Velocity Values

Nitta (1977) utilized upper air observations of seven U.S.S.R. ships stationed within the GATE A/B-scale array to derive a time

a) Areal coverage of shipboard radar during the analysis period

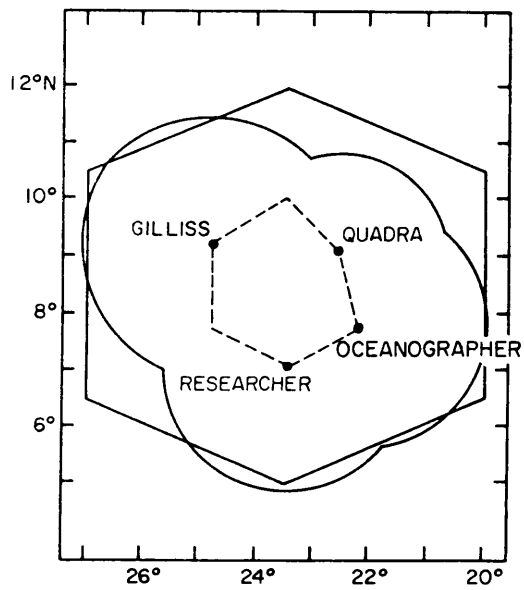

b) GATE master radar array

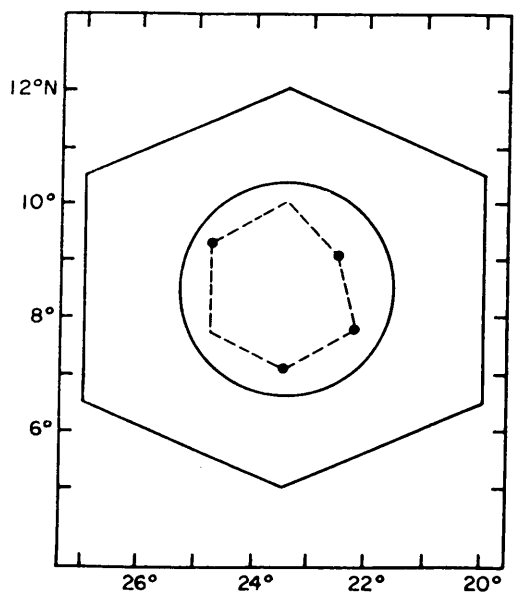

Figure 4. Depiction of areal coverage of a) the shipboard radar shown in the photomosaics of Arkell and Hudlow (1977) during the analysis period, and b) the GATE master radar array. The solid hexagon (——) represents the A/B-scale array and the dashed hexagon (---) represents the B-scale array.

series depiction of the mean vertical motion profile ($\overline{\omega}_{AB}$) during a portion of the lifetime of the 4-6 September cloud cluster. The $\overline{\omega}$ is determined by

$$\overline{\omega} = \overline{\omega}_s - \int_{p_s}^{p} \overline{\nabla \cdot \mathbb{V}}\, dp \qquad (1)$$

where $\overline{\Delta \cdot \mathbb{V}}$ is the horizontal divergence and p_s is surface pressure. The p-velocity at the surface, ω_s is determined by

$$\overline{\omega}_s = \frac{\partial \overline{p}_s}{\partial t} + \overline{\mathbb{V}_s \cdot \nabla p_s} \qquad (2)$$

where $\mathbb{V}_s$ corresponds to the surface wind. A top boundary condition derived from the first law of thermodynamics assumes that radiation is the sole diabatic input in the uppermost layer (100-125 mb), hence

$$\overline{\omega}_t \quad (p = 112.5 \text{ mb}) = \left(\frac{\frac{\partial \overline{\theta}}{\partial t} + \overline{\mathbb{V} \cdot \nabla \theta} - \frac{(p_o/p)^K}{c_p} Q_R}{\partial \overline{\theta}/\partial p} \right)_{p = 112.5} \qquad (3)$$

where c_p represents specific heat of air at constant pressure, $K = R/c_p$, and Q_R denotes radiational heating from Dopp'ick (1972). Then a correction is applied to the $\overline{\omega}$ values computed by Eq. (1) by linearly adjusting $\nabla \cdot \mathbb{V}$ with height so as to be in agreement with the $\overline{\omega}_+$ condition. The temporal and vertical resolutions for the $\overline{\omega}$ computations are 3 hours and 25 mb, respectively. Estimations of $\overline{\omega}_{A/B}$ profiles

are derived from the graphical time series depiction of Nitta (1977) and are used as inputs for the radiative $\bar{\omega}$ model discussed in the analysis section.

IV. ANALYSIS

4.1 Slab Analysis

An analysis of the radiative convergence field was performed for the 225 boxes of the array by Cox and Griffith (1978). This so-called "slab" analysis involves dividing the troposphere into three 300 mb thick layers and analyzing the radiative convergence field for each layer. This analysis is carried out for five 6 hour time intervals from 1800 LST on 4 September to 0000 LST on 6 September. So that areas of active convection may be easily interpreted, radar echo fields (Arkell and Hudlow, 1977) from within each time period are superimposed on the radiative divergence analysis. Figures 5-9 show the time series analysis of the evolution of the radiative convergence fields and the precipitation field during the cloud cluster life cycle. Parts a, b, and c of each figure show the radiative convergence fields for the 100-400 mb, 400-700 mb and 700-1000 mb layers, respectively. Latitude corresponds to the ordinate and longitude to the abscissa in each figure.

Figure 5a-c shows the net radiative convergence fields for 1800-2400 LST 4 September 1974. Most of the active convection is occurring in the area centered at 7.5°N - 25°W and corresponds to the dissipating squall line system of 4 September documented by Houze (1977). To the north of the squall line system, isolated small echo regions are observed, indicating the formative stages of the double cloud cluster system of 5 September. Most noteworthy is the observation that the largest gradients in horizontal radiative convergence seem to occur in the 400-700 mb layer. The smallest gradients in radiative

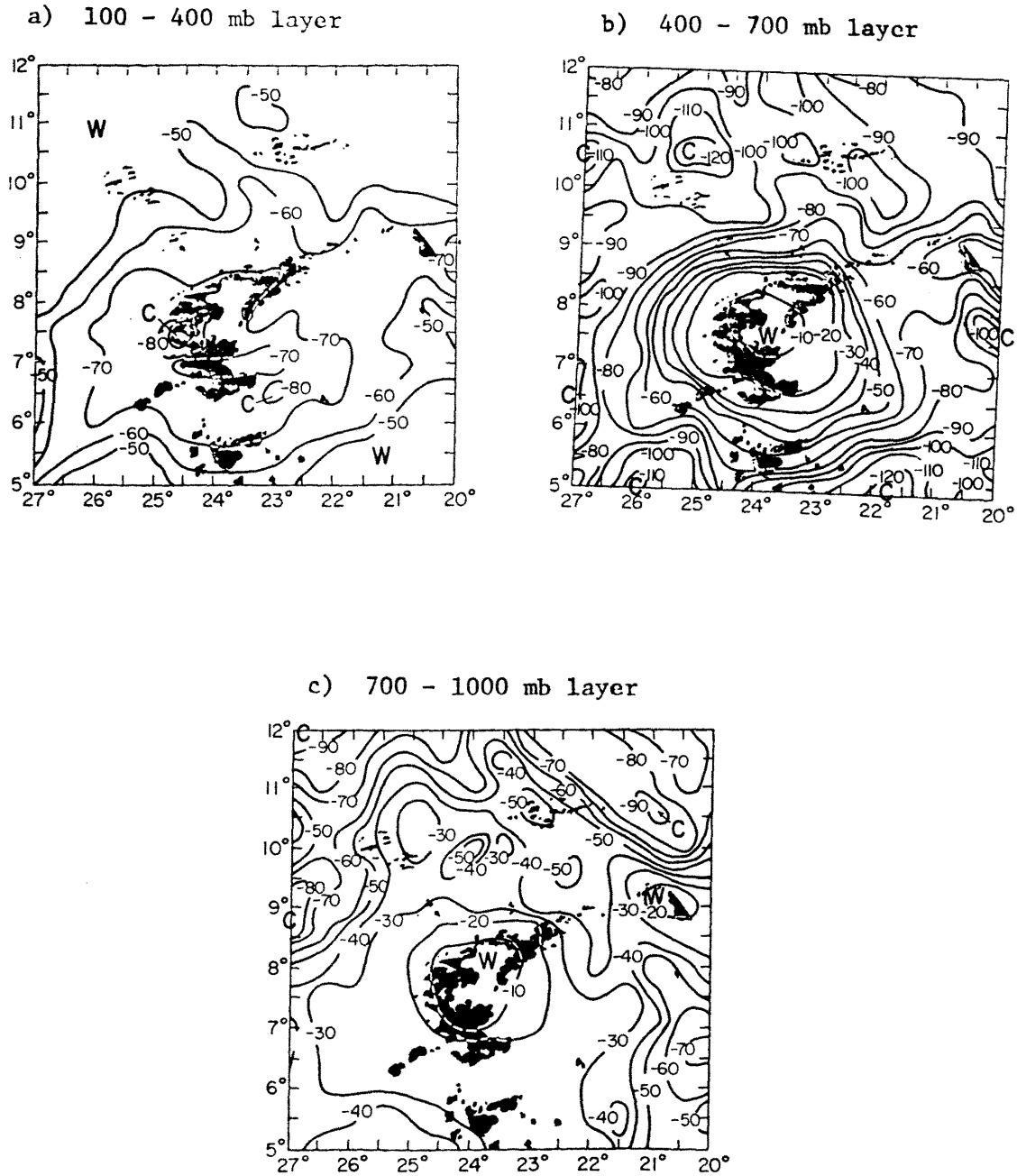

Figure 5. A latitude versus longitude "slab" view of the 1800-2400 LST total (SW + LW) convergence over the A/B-scale array on 4 September 1974. The shaded area constitutes the 2230 LST radar echo area from Arkell and Hudlow (1977). The "C" denotes areas of maximum radiative cooling while the "W" denotes areas of minimum radiative cooling. Units are in Wm^{-2} 300 mb^{-1}.

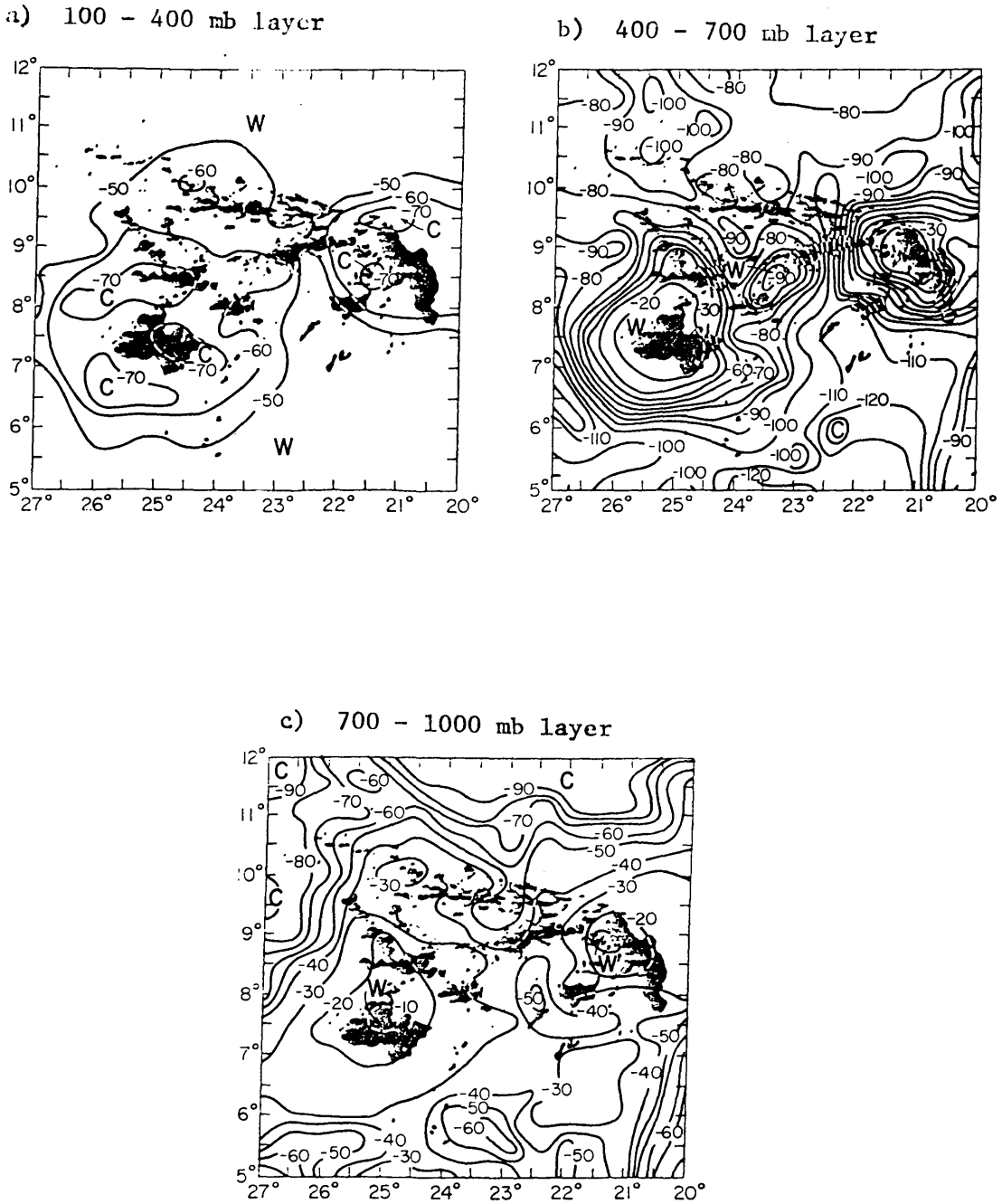

Figure 6. Same as Figure 5 except for 0000-0600 LST on 5 September 1974 convergence and 0430 LST radar.

a) 100 - 400 mb layer

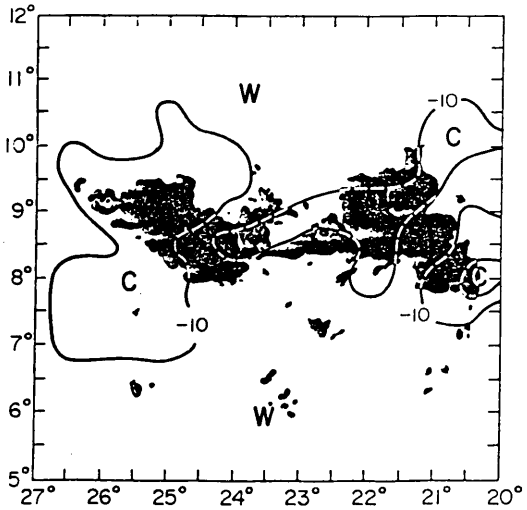

b) 400 - 700 mb layer

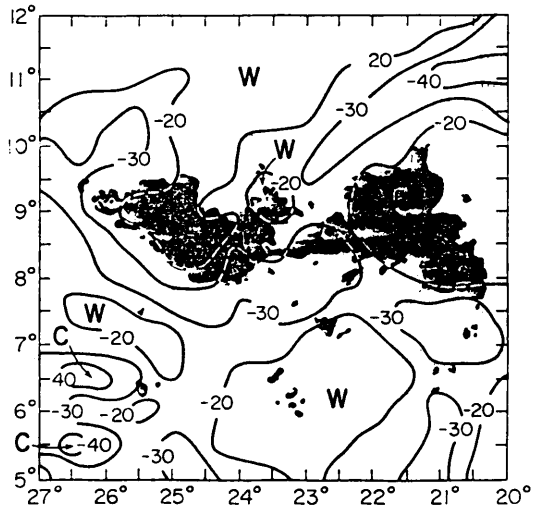

c) 700 - 1000 mb layer

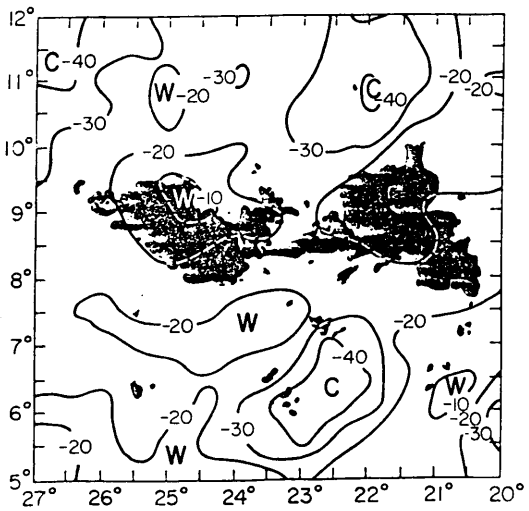

Figure 7. Same as Figure 5 except for 0600-1200 LST on 5 September 1974 convergence and 1030 LST radar.

a) 100 - 400 mb layer

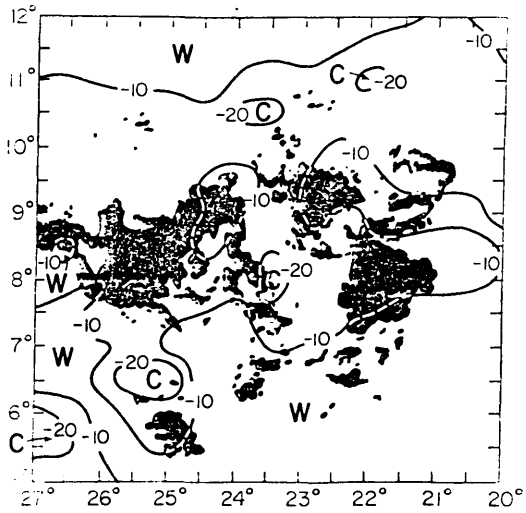

b) 400 - 700 mb layer

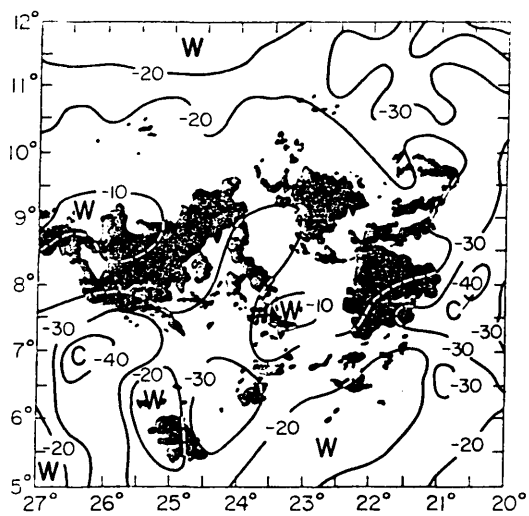

c) 700 - 1000 mb layer

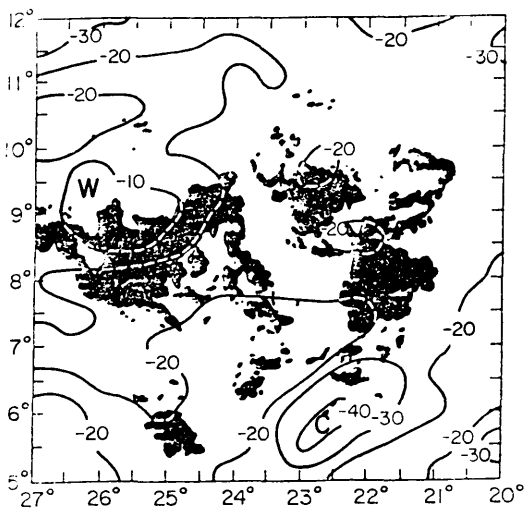

Figure 8. Same as Figure 5 except for 1200-1800 LST on 5 September 1974 convergence and 1630 LST radar.

a) 100 - 400 mb layer

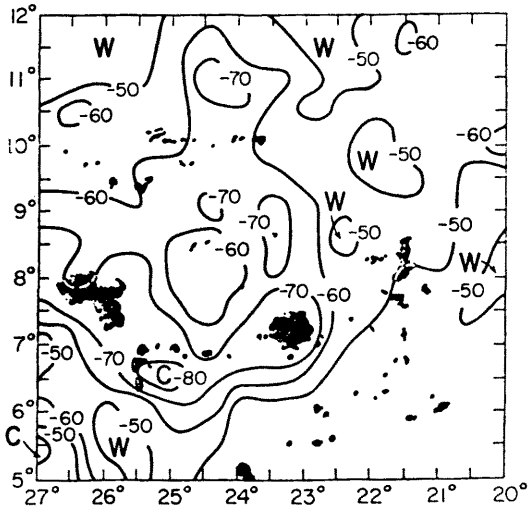

b) 400 - 700 mb layer

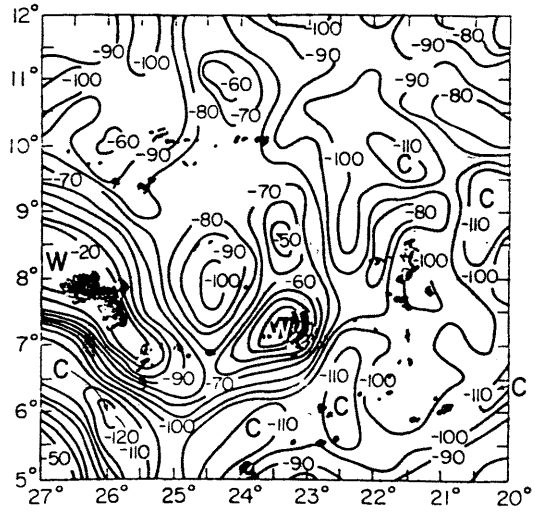

c) 700 - 1000 mb layer

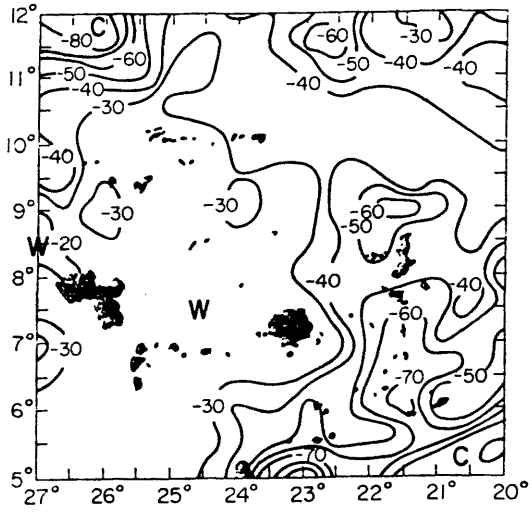

Figure 9. Same as Figure 5 except for 1800-2400 LST on 5 September 1974 convergence and 2230 LST radar.

convergence are observed in the 100-400 mb level. Gradients at the 700-1000 mb level tend to have magnitudes somewhere in between those of the middle and upper layers. The strongest gradients occur in middle levels and the weakest gradients are found in the upper levels; this arrangement is characteristic of all time periods and is in general agreement with the findings of Cox and Griffith (1978).

The areas of greatest radiative forcing which correspond to areas of strongest gradients of radiative convergence seem to be well correlated with the regions of active convection, as indicated by the 0000 GMT (2230 LST) radar. In the 100-400 mb layer, largest radiative energy losses occur over the convective region, the result of large radiative cooling at high cloud top levels within the active region. The gradient is reversed in the two lower layers, with smaller radiative energy losses occurring in the regions of active convection. The high clouds in the active region tend to suppress LW radiative losses at lower levels. In contrast, the surrounding areas, with lower cloud tops and clear areas, experience much larger radiative cooling.

Turning to the formative region of isolated echoes to the north of the dissipating squall line system, an interesting reversal in gradient is observed between the 1000-700 mb layer and the 400-700 mb layer. Large radiative energy losses relative to the surrounding areas occur in the 400-700 mb layer, due to strong radiative cooling from middle cloud top levels in this isolated echo region. However, radiative cooling in the lowest layer is suppressed relative to the surrounding region by the presence of middle clouds.

Figure 6a-c shows the evolving radiative convergence field for the following 6 hour period, 0000-0600 LST on 5 September. The radar field

for 0600 GMT (0430 LST) is superimposed upon the radiative divergence field. The northern area of isolated precipitation echoes at 2230 LST has expanded considerably by 0430 LST. The associated net radiative convergence fields show the development of several distinct features. The radiative convergence gradients have strengthened over those of the period before and are sharpest in the region of 6-10°N in an E-W elongation across the analysis area. The east-west orientation of the isopleths and the associated cloud field suggest the predominance of meridional radiative forcing upon the cloud cluster system. Two distinct areas of large convergence gradients do appear to exist at all levels, one centered at 7.5°N, 25°W and the other at 9°N, 21.5°W. This may be readily associated with the double cluster appearance of the system in IR satellite imagery during disturbance intensification.

It is worth noting that a gradient reversal has taken place in the 400-700 mb layer over the formerly isolated echo region of the previous time period. Apparently, with the intensification of convection and expansion of precipitation within the region, more cloud tops have penetrated the 100-400 mb layer. This acts to suppress LW radiative cooling in the 400-700 mb level relative to the cooling observed in the non-convective surroundings. The precipitation region now exhibits suppressed radiative cooling in the lower two layers and enhanced radiative cooling in the upper layer, when compared to the surrounding region.

The cluster system undergoes further intensification, approaching the mature stage during the 0600-1200 LST period depicted in Figure 7a-c. The precipitation pattern on the 1030 LST radar is characterized by a concentration of a broad echo regime extending east to west

between 8° and 10°N across the analysis area. Two distinct centers in echo activity appear, one at 8.5°N, 24.5°W and the other at 9°N, 21.5° W. The most striking feature of the total radiative convergence field during the 0600-1200 LST period is the dramatic weakening of gradients relative to the previous period. Having now reached the daytime period, solar energy input in the form of SW radiative warming tends to counterbalance somewhat the LW cooling of the troposphere, resulting in the weakening of radiative convergence gradients between the cluster and its surrounding environment.

The distinct double structure previously evident in the radiative convergence fields is not as readily apparent in the 0600-1200 LST period. Although gradients are generally more poorly defined than in previous time periods, no reversals seem to have taken place in any layer. In a similar "slab" analysis, Cox and Griffith (1978) reported a reversal of radiative convergence gradients for all layers during a four hour period centered on 1200 LST 5 September. The gradient reversal is only observable for the few hours about solar noon when SW warming dominates over LW cooling. The two daytime 6 hour averaging intervals in this study separated at solar noon, tend to smooth out the solar forcing to the extent that the gradient reversal is not observed. Although no net radiative warming is observable in any of the 300 mb thick layers, some warming is found in individual 100 mb layers. This will become more apparent in the cross section analyses of the following section.

In the 1200 - 1800 LST period, shown in Figure 8a-c, the cluster system passes from the mature stage into the dissipating stage, characterized by the slow breakup and diffusion of organized precipitation

areas indicated by the 1630 LST radar. The radiative convergence field is qualitatively similar to that of the previous period. If there is a difference from the morning period, it is that the radiative energy gradients are even more diffuse, with little gradient organization between the cloud cluster and its surrounding environment. The strong meridional structure of forcing so evident in the nighttime periods is virtually nonexistent in the 1200-1800 LST period.

The 1800-2400 LST 5 September period of Figure 9a-c, reveals a significant decay in the precipitation area with only two small areas of organized precipitation evident on the 2230 LST radar. The first area is centered at about 7.5°N and 26°W and appears to be propagating eastward out of radar range. The second is located at roughly 75°N, 23°W. Having reached the nighttime period, the lack of SW heating brings about a significant increase in the radiative convergence gradients over those of the previous period. However, the only area of concentrated forcing seems to be in the vicinity of the two organized precipitation areas and only in the 400-700 mb layer. Even so, the gradients are far less organized than in the previous two nighttime periods. Apparently, the more diffuse nature of the cloud top structure and associated radiative convergence fields is a result of many cloud remnants of active convection. These clouds are found predominantly at low and middle tropospheric levels, since many high cloud remnants have either dissipated or have been advected out of the analysis area by stronger easterly flow at upper levels. Consequently, the only strong radiative forcing is associated with the small areas of active convection where high clouds suppress radiative losses at middle levels.

It is perhaps helpful to summarize the findings of the "slab" analysis. At the formative stage (1800-2400 LST 4 September), isolated radar echoes are located predominantly below middle cloud top regions. There results a radiative convergence gradient reversal from the 700-1000 mb layer to the 400-700 mb layer. The formative convective area middle cloud top regime results in enhancement of LW cooling in the middle (400-700 mb) layer and a suppression of LW cooling in the lower (700-1000 mb) layer, relative to surrounding regions. The 100-400 mb radiative convergence field remains essentially undisturbed.

During the intensification stage (0000-0600 LST), cloud top penetration into the 100-400 mb layer is achieved in the newly formed convective area. This results in a gradient reversal at 400-700 mb with high clouds now suppressing LW cooling at the middle levels relative to the surrounding environment. Radiative cooling is enhanced compared to the surrounding area at high cloud top levles in the 100-400 mb layer. A meridional radiative forcing is also evident across the analysis area.

The system approaches maturity during the 0600-1200 LST period. Since SW heating is now at least in part compensating the LW cooling, the gradients in radiative divergence between the cluster and its surroundings are considerably weakened. The large time averaging interval and significant vertical thickness of the layers tend to suppress the effect of strong solar forcing about solar noon. Consequently, the gradient reversal within this system observed by Cox and Griffith (1978) is not detectable in the "slab" analyses.

As the system begins to dissipate during the 1200-1800 LST period, gradients in radiative convergence become still more diffuse. As

nighttime descends upon the dying cluster, radiative convergence gradients are once again enhanced due to the absence of SW heating. The strong forcing is confined to the 400-700 mb layer and to very localized areas of active convection. During the final two periods, the surrounding area has a very diffuse radiative convergence field, with enhanced cooling due to middle cloud top remnants of active convection. The high cloud top remnants appear to have dissipated or advected eastward out of the analysis area in the stronger flow at upper tropospheric levels.

4.2 Cross Sections

To further evaluate radiative forcing on the 5 September cloud cluster, vertical cross sections are constructed for each of the five 6 hour time periods in the disturbance life cycle. Meridional radiative forcing is assessed through interpretation of north-south (N-S) cross sections along latitude 23.5°W. Zonal radiative forcing is evaluated through analysis of east-west (E-W) corss sections along longitude 8.5°N.

Both the N-S and E-W cross sections extend the width of the Cox, Griffith array, each encompassing fifteen 1/2° x 1/2° boxes. The locations of the zonal and meridional cross sections are chosen so that their common point, 8.5°N, 23.5°W, occurs at the center of the analysis region. Each cross section extends vertically from 1000-100 mb and is resolved into nine 100 mb layer radiative convergence averages for each 1/2° x 1/2° box.

Figure 10-14 show the time series evolution of the radiative convergence fields in vertical cross section form. Each figure contains

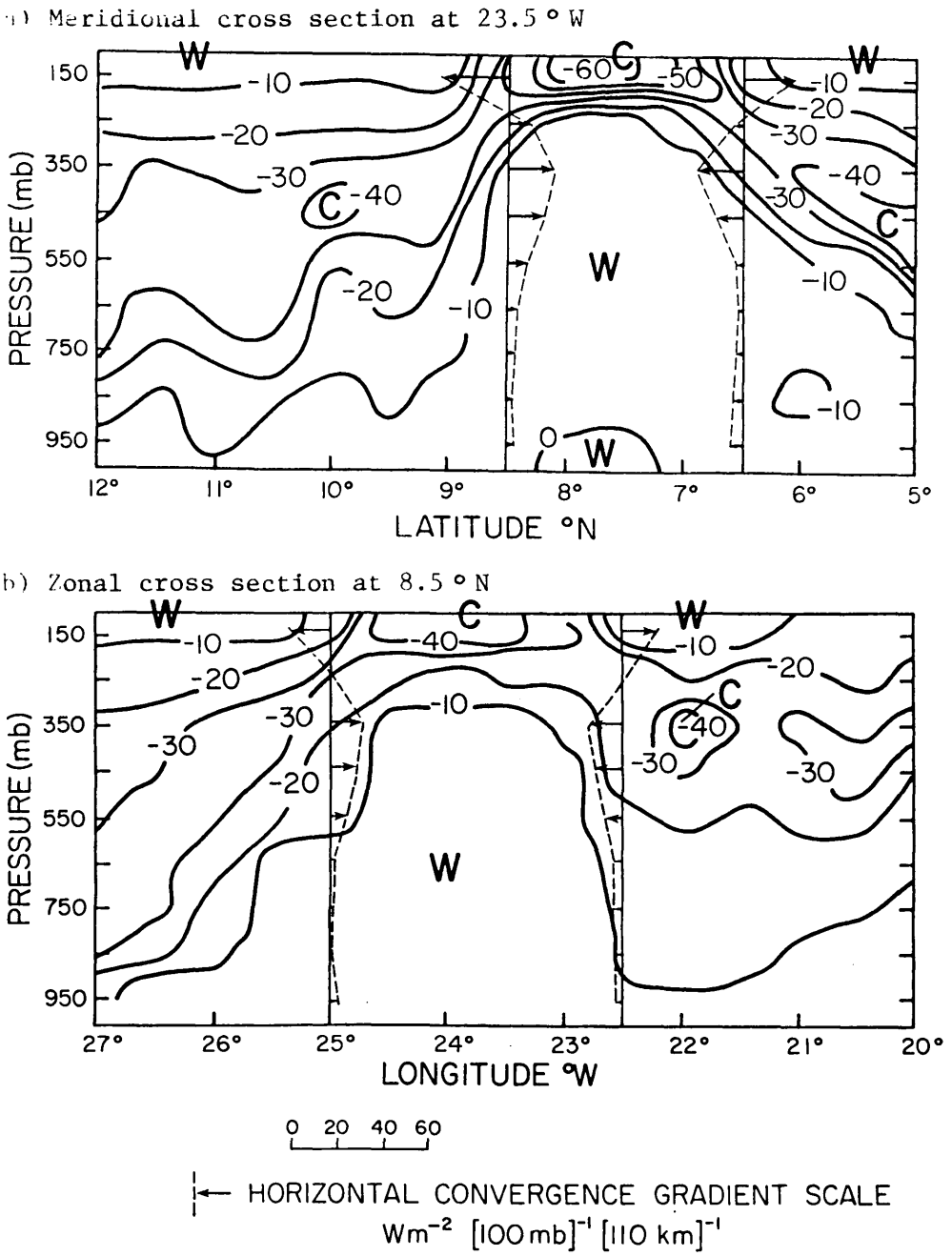

Figure 10. A pressure vs. a) latitude (at 23.5°W), and b) longitude (at 8.5°N) cross sectional view of the A/B-scale array for 1800-2400 LST on 4 September 1974. The radiative convergence units are in Wm^{-2} $(100\ mb)^{-1}$. The magnitude and direction of horizontal radiative convergence gradients are shown in areas of concentrated radiative forcing. The arrows point towards regions of smaller radiative cooling and are analogous to the hypothesized inflow-outflow regimes of Gray (1979a) shown in Figure 2.

a) Meridional cross section at 23.5°W

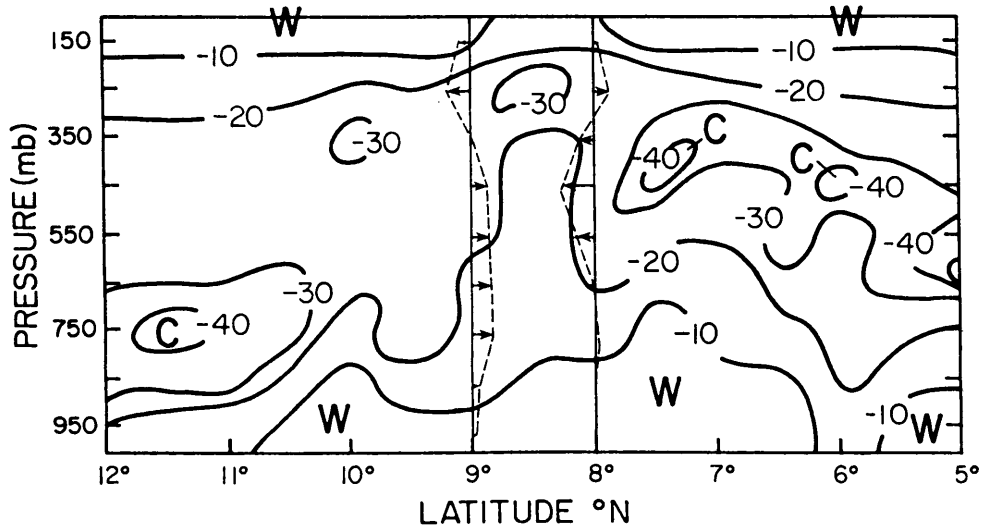

b) Zonal cross section at 8.5°N

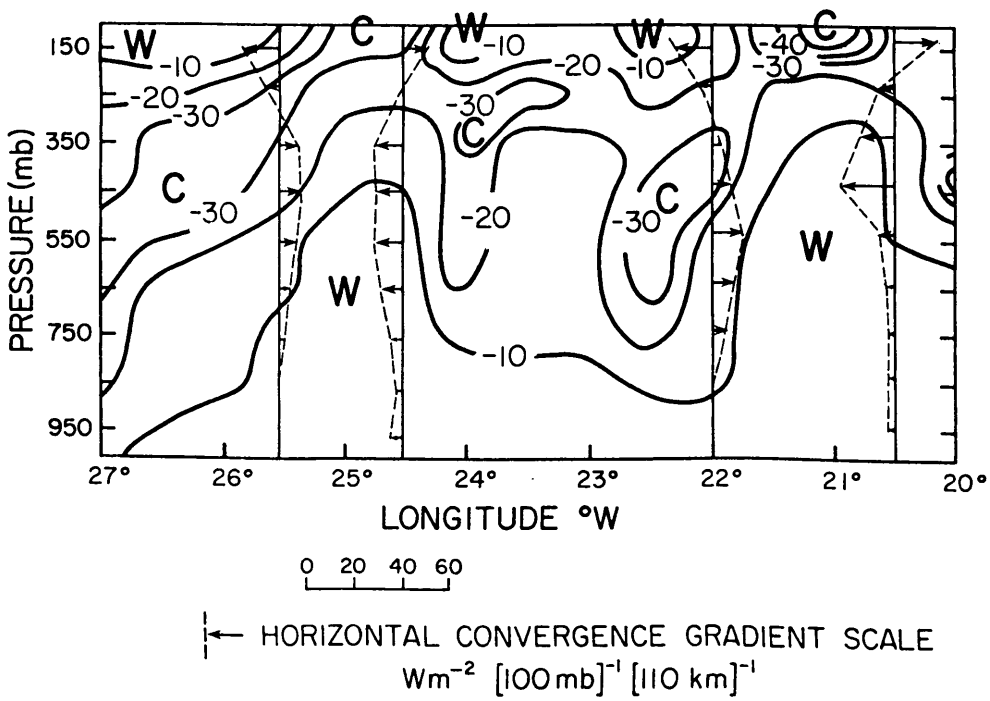

Figure 11. Same as Figure 10 except for 0000-0600 LST on 5 September 1974.

a) Meridional cross section at 23.5°W

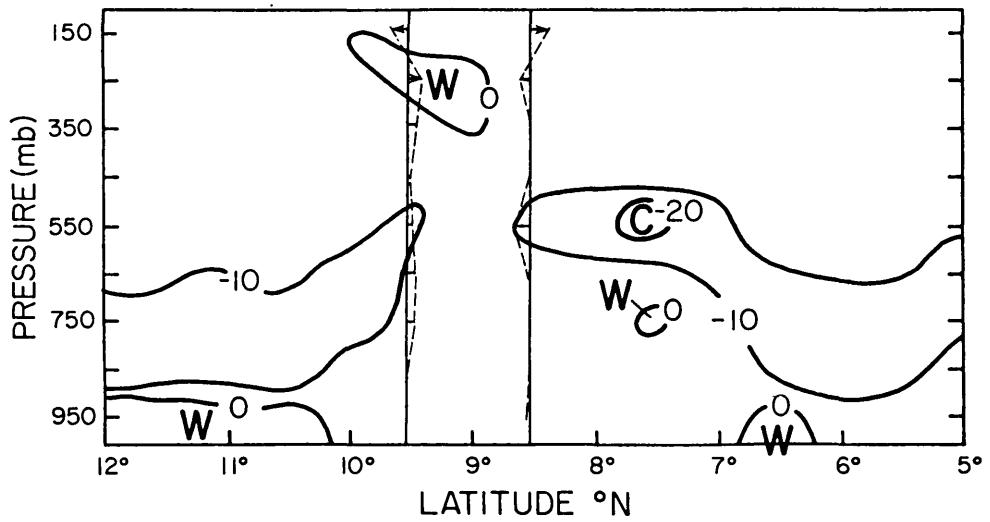

b) Zonal cross section at 8.5°N

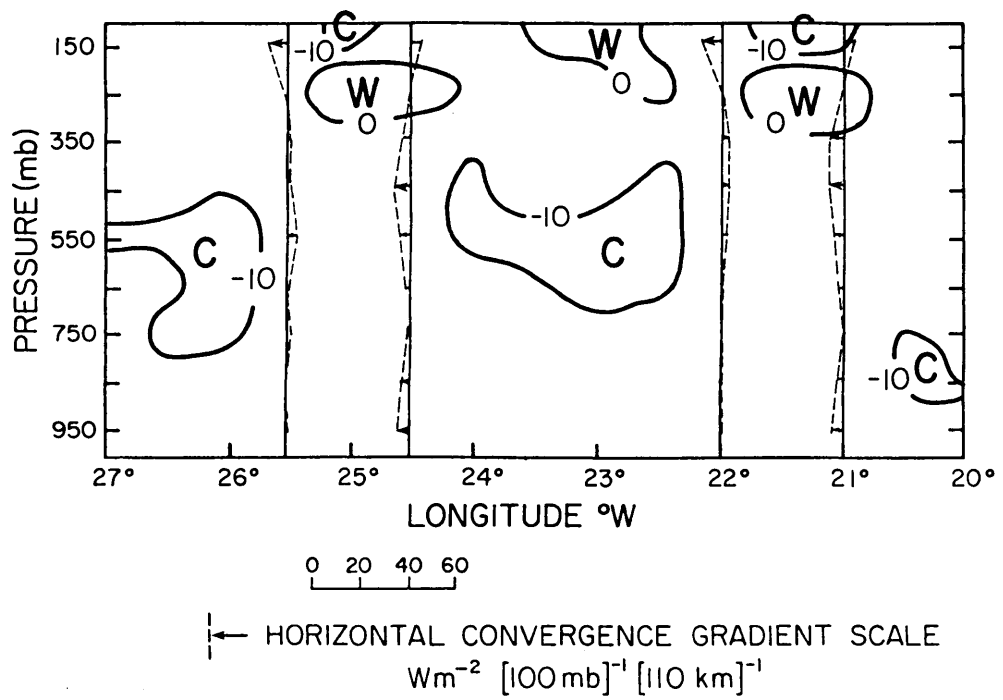

Figure 12. Same as Figure 10 except for 0600-1200 LST on 5 September 1974.

a) Meridional cross section at 23.5 ° W

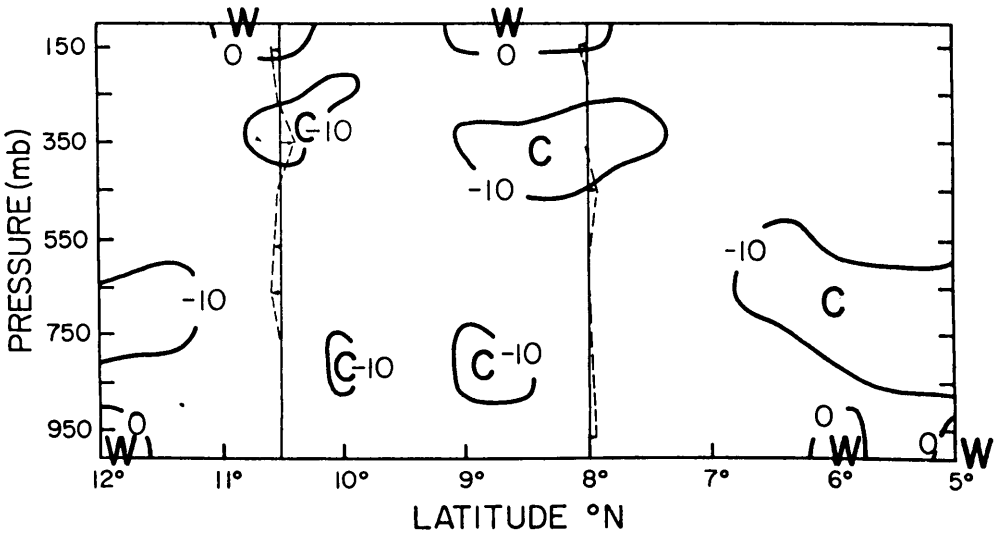

b) Zonal cross section at 8.5 ° N

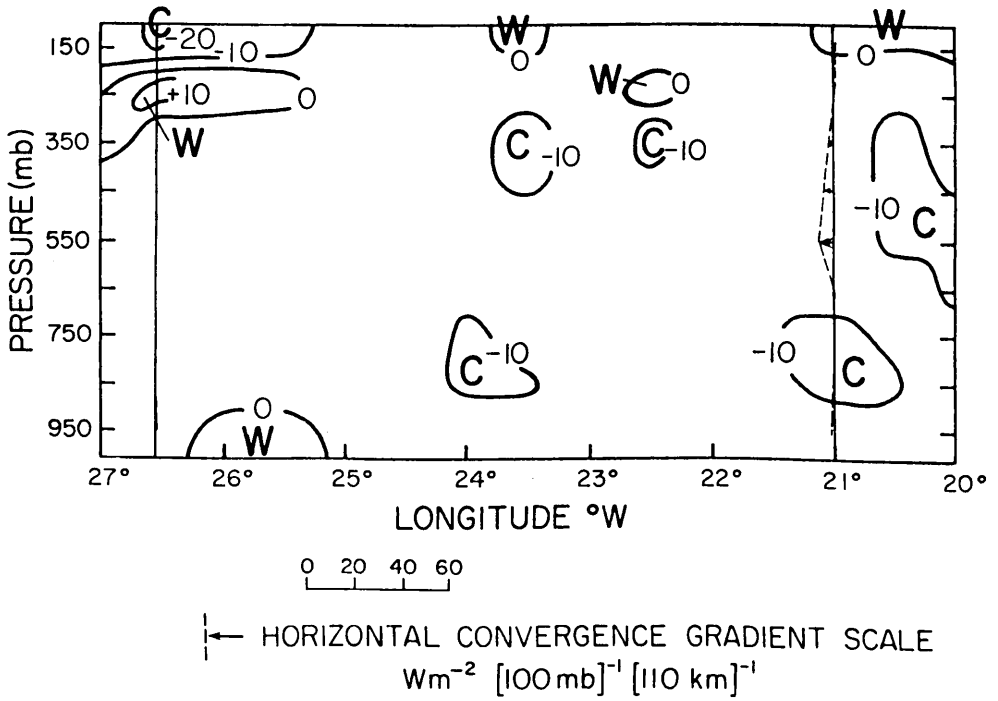

Figure 13. Same as Figure 10 except for 1200-1800 LST on 5 September 1974.

a) Meridional cross section at 23.5 ° W

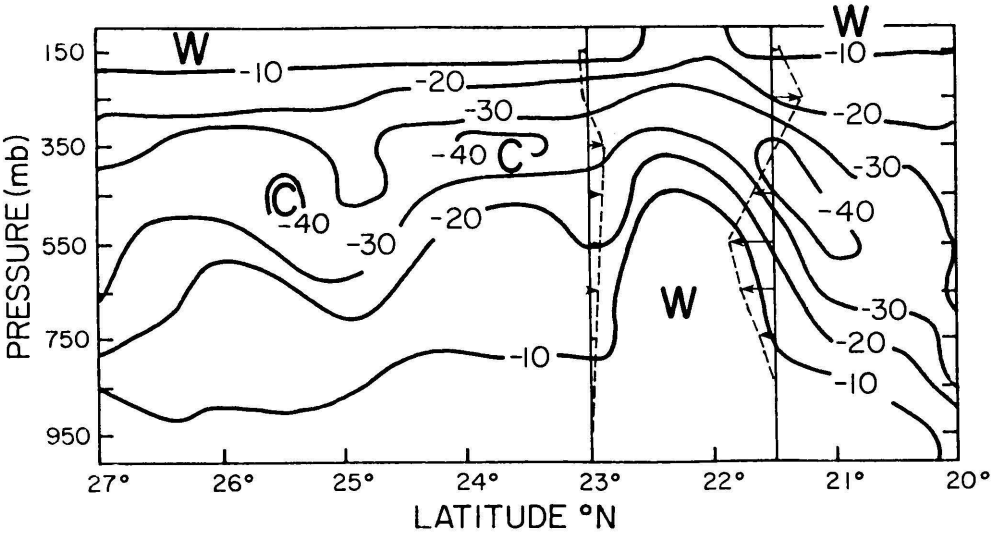

al cross section at 8.5 ° N

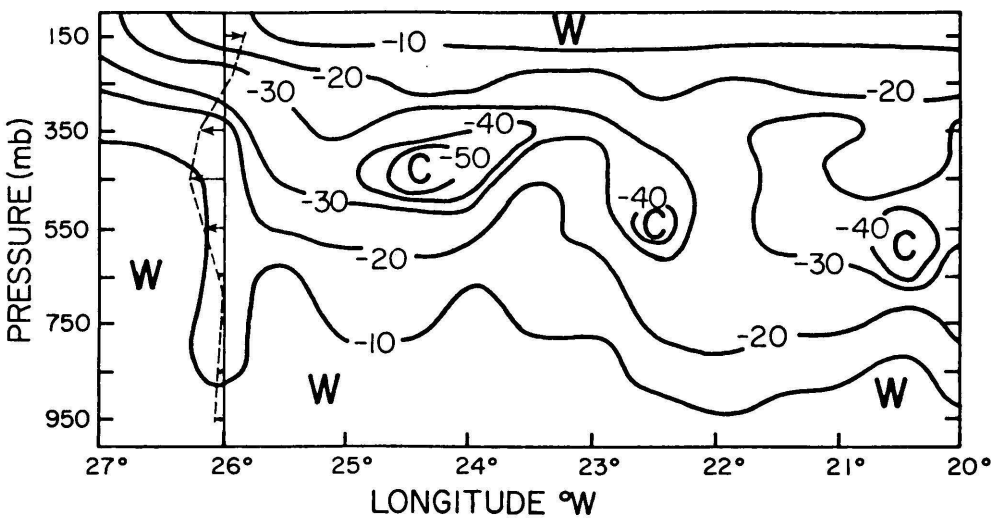

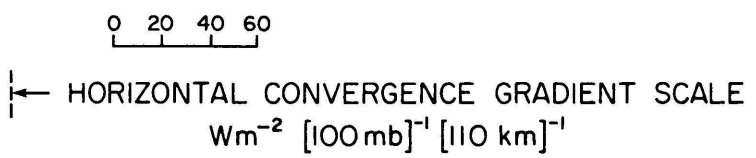

Figure 14. Same as Figure 10 except for 1800-2400 LST on 5 September 1974.

two parts; Part a is the meridional cross section along 23.5°W, while Part b involves the zonal cross section along 8.5°N. The ordinate of each diagram is pressure while the abscissa corresponds to latitude or longitude. In addition, horizontal radiative convergence gradients are depicted at several points, with the arrows pointing toward regions of greater radiative convergence (lesser radiative divergence). The arrows are pointed in this way to be consistent with the hypothesized inflow-outflow regimes discussed by Gray (1979a) and shown in Figure 2.

Figure 10a-b shows the meridional and zonal cross sections for the initial 1800-2400 LST period of 4 September. The radiatively active disturbance area is clearly defined on both the meridional and zonal cross sections. This area of relatively large radiative forcing corresponds to the dying squall line system of 4 September as discussed by Houze (1977). The most significant horizontal radiative forcing appears confined to the middle and upper levels above 500 mb. Typical horizontal radiative convergences are on the order of 15-60 Wm^{-2} $(100\ mb)^{-1}$ over a 110 km distance. Once again, the presence of high clouds in the disturbance region leads to enhanced LW cooling, primarily in the 100-200 mb layer relative to the surrounding environments. High cloud suppression of LW cooling results in a reversal in horizontal radiative convergence gradients with larger LW cooling in surrounding areas in the layers below 200 mb. There are apparently enough middle clouds to suppress LW radiative cooling in the lowest layers of the region surrounding the disturbance as well. As a result, horizontal gradients in radiative convergence between the convective system and its surroundings are weakened considerably in the layers

below 500 mb. Horizontal gradient values in these lower layers typically range from 2 to 10 Wm^{-2} $(100\ mb)^{-1}$ over a 110 km distance. The generally weak horizontal gradients in the radiative convergence for the lower levels are a general characteristic found in the vertical cross sections throughout the cloud cluster lifetime. Interesting to note is the radiative warming occurring in the 900-1000 mb layer (cloud base region) at the 7.5 - 8.0°N region of the meridional cross section in Part a of Figure 10.

The only hint of radiative forcing associated with the newly developing convective area farther to the north appears to be a kinking of the isopleths around 10°N in Figure 10a. The stronger radiative cooling at middle cloud top levels of this region tends toward a reversal of the middle level horizontal radiative convergence gradients relative to the well developed convective system. This is in qualitative agreement with the observation of radiative forcing in the initial convective period as discussed previously in the "slab" analysis section.

Figure 11a-b shows meridional and zonal cross sections of the cloud cluster during its intensification stage in the 0000-0600 LST period on 5 September. The meridional cross section in Figure 11a indicates an area of enhanced radiative forcing between 8° and 9°N. Once again, the strongest forcing is observed at middle and upper levels but is somewhat smaller in magnitude and over a considerably smaller horizontal domain than in the previous period. Typical horizontal radiative convergence gradients are on the order of 10-30 Wm^{-2} $(100\ mb)^{-1}$ over a 110 km distance. The smaller magnitude and horizontal domain of radiative forcing is in part a result of the cross

sectional location. By 0430 LST, the developing disturbance has assumed a double cluster appearance, and the cross section along 23.5°W latitude runs through the less intense area between the two convectively active regions. Nevertheless, a significant amount of meridional radiative forcing is observable in this region of lesser intensity.

Perhaps more noteworthy is the E-W cross section shown in Figure 11b. Here, the double cloud cluster characteristic is readily apparent in the gradients of horizontal radiative convergence. Middle and upper level horizontal gradients are on the order of 15-40 Wm^{-2} per 100 mb over a 110 km distance, with weaker gradients at lower levels. These values are slightly larger than those observed on the meridional cross section and are similar to those observed in the previous time period.

A dramatic change in the radiative convergence pattern is apparent in the cross sections for the 0600-1200 LST period shown in Figure 12a-b. As the disturbance matures, a significant weakening in gradients of radiative convergence occurs in much the same fashion as observed in the "slab" analysis. The presence of SW warming superimposed upon the LW cooling acts to weaken these horizontal gradients between the cluster and its surroundings, as discussed previously. In fact, the gradients of net radiation were weak enough that the vertical profiles of LW convergence were consulted in order to better define the areas of active radiative forcing. Horizontal gradients in radiative convergence are in the range of 0-13 Wm^{-2} $(100\ mb)^{-1}$ over a 110 km distance. Even in individual 100 mb intervals, there seems to be little indication of a reversal of horizontal radiative convergence gradients relative to the nighttime cases. Once again, this appears to

differ somewhat with the findings of Cox and Griffith (1979), for reasons noted previously.

Two regions of radiative warming appear in the 0600-1200 LST cross sections. Warming of as much as 5 Wm^{-2} $(100\ mb)^{-1}$ over a 110 km distance is observable in the upper levels of the disturbed regions. Strong SW convergence dominates over large LW divergence values in the vicinity of high cloud tops. Another region of local radiative warming occurs in the 900-1000 mb layer outside of the disturbed area. The SW convergence coupled with suppressed LW divergence at cloud base levels is sufficient to produce these localized warming regions.

During the 1200-1800 LST period, the cluster system reaches full maturity and begins slow dissipation. The cross sections of Figure 13a-b show the nearly total collapse of organized radiative forcing upon the convective region. The horizontal radiative convergence gradients depicted on both cross sections are weak and disorganized, with values typically in the range of 0-10 Wm^{-2} $(100\ mb)^{-1}$ over a 110 km distance. It is evident from the satellite imagery that, as the mature system begins to dissipate, the well-defined cluster boundaries observable in the intensifying stages of the convective cycle no longer exist. During the mature and dissipation stages, cirrus blow-off and middle cloud remnants of previous convection tend to make system boundaries more diffuse, resulting in less concentrated horizontal gradients of radiative convergence. This is especially evident in the zonal cross section, with the collapse of the double region of radiative forcing, despite evidence that two clearly defined convective areas remain evident on the 1630 LST radar (Figure 8). The meridional cross section in Figure 13a shows some reversal of horizontal radiative

convergence gradients at middle levels at 8°N, which shows agreement with the observations of daytime radiative forcing by Cox and Griffith (1978).

As in the previous period, local areas of radiative heating are observed in the upper layers in the disturbed regions and in the lowest layer at cloud base level in regions surrounding the cluster.

The rapidly dissipating cloud cluster of the 1800-2400 LST period shown in Figure 14a-b is marked by an intensification of horizontal radiative convergence gradients in the absence of SW warming. However, the observed gradients are not nearly as intense as the horizontal gradients of the previous nighttime periods. Typical values of horizontal radiative forcing are on the order of 5-25 Wm^{-2} $(100\ mb)^{-1}$ over a 110 km distance at middle and upper levels, with lesser values below. Figure 14b contains only one depiction of the E-W radiative forcing (26°W), since only the eastern part of the convective disturbance remains in the analysis area at 8.5°N.

Again, the increasingly disorganized nature of the radiative forcing upon the cloud cluster system is readily apparent. The lack of a concentrated horizontal gradient in radiative convergence is attributable to the increasingly diffuse nature of the system boundaries brought about by inactive cloud remnants from former convection. Much of the high cloudiness associated with the disturbance has dissipated or has been advected eastward out of the analysis area, resulting in the observation of smaller radiative cooling at upper levels in the cross sections.

Table 1 provides a simplifed summary of the meridional and zonal radiative forcing apparent in the vertical cross sections during the

TIME PERIOD (LST)	CLUSTER MINUS CLEAR TTC EAST-WEST (8.5°N)	NORTH-SOUTH (23.5°W)
4 September 1800-2400	63.0	61.9
5 September 0000-0600	63.9	45.3
0600-1200	28.5	16.0
1200-1800	10.8	-10.3
1800-2400	43.9	36.1

Table 1. Cluster minus clear difference in total tropospheric convergence (TTC) for the cluster life cycle. Units are in Wm^{-2} $(900\ mb)^{-1}$. The differences apply over a 110 km horizontal distance and are derived from the north-south and east-west cross sections.

cloud cluster life cycle. The table compares the mean cluster versus surrounding area difference in total (SW + LW) tropospheric (100-1000 mb) radiative convergence (TTC) from the selected depictions of horizontal gradients on the vertical cross sections. Cox and Griffith (1978) indicate that larger negative values of nocturnal TTC occur in the suppressed or surrounding regions due to increased LW losses to space relative to the disturbed region. In contrast, the daytime TTC values are remarkably constant throughout Phase III of GATE. Table 1, with positive values indicating larger total tropospheric cooling occurring outside the cluster region, seems to bear this out.

It is evident that strong radiative forcing occurs during the initial nighttime periods (1800-0600 LST, 4-5 September), with the radiative forcing of the 1800-2400 LST period dominated by the decaying squall line system. The 0000-0600 LST period shows a substantial weakening of the radiative forcing, due to SW warming superimposed upon the LW cooling. As the cluster boundary regions become more diffuse due to cirrus blow-offs and assorted middle cloud convective remnants, the gradients become even weaker during the 1200-1800 LST period. A reversal of the horizontal radiative convergence gradient at middle levels comparable to that observed by Cox and Griffith (1978) dominates the TTC mean in the meridional cross section during this late afternoon period. The forcing increases somewhat in the final 1800-2400 LST period; however, not to the extent observed during previous nighttime periods.

During the analysis period, E-W forcing is slightly larger in magnitude than the N-S forcing. However, due to the dependence of the analysis on the placement of the vertical cross sections, no conclusive

evidence exists that proves the E-W forcing is actually greater. In fact, the primary component of radiative forcing is likely to be N-S forcing, due to the east to west elongation of the disturbance system. It is important to note that the TTC analysis does indicate that the E-W radiative forcing is comparable to the N-S radiational forcing over localized regions of interest.

4.3 The Radiatively Derived Vertical Motion Model

In a further attempt to assess the effects of radiative forcing upon cluster- and large-scale dynamical interactions, a vertical motion model is constructed. A daytime (0600-1200 LST, 5 September) and a nighttime (1800-2400 LST, 5 September) period within the cloud cluster life cycle are considered. Nitta (1977) provides time series vertical velocity estimates for the A/B array, which are the bases for the cloud cluster vertical motion calculations. A discussion of the methodology for determination of the $\bar{\omega}_{A/B}$ profiles appeared previously in Chapter 3. The net upward motions observed for both the 0600-1200 LST and 1800-2400 LST cases were indicative of the convective activity within the array. However, the cloud cluster occupied only a portion of the A/B array; therefore, we next devise a method in which Nitta's $\bar{\omega}$ values may be used to calculate cloud cluster vertical motion.

4.3.1 Methodology

Given the vertical motion profile ($\bar{\omega}_{A/B}$) from Nitta (1977), the A/B array is treated as a system which is mass balanced by the following expression:

$$\bar{\omega}_{A/B} A_{A/B} = \bar{\omega}_{up} A_{up} + \bar{\omega}_{down} A_{down} \qquad (4)$$

where $A_{A/B}$ is the area of the A/B array; $\bar{\omega}_{up}$ is the mean vertical motion in the convective region; A_{up} is the area of the convective region; $\bar{\omega}_{down}$ is the mean vertical motion in the subsidence region; and A_{down} is the area of the subsidence region $(A_{A/B} - A_{up})$. In the equation above, $A_{A/B}$ is known, and A_{up} may be determined from IR satellite imagery. The imagery from 0900 LST and 2100 LST was used to subjectively determine the cluster area within the A/B array. These times were chosen since they constituted the midpoints of the daytime (0600-1200 LST) and nighttime (1800-2400 LST) periods of interest. A_{down} is simply the difference $(A_{A/B} - A_{up})$. There remain two unknowns, $\bar{\omega}_{up}$ and $\bar{\omega}_{down}$, which may be obtained in the following manner.

A major portion of the compressional warming in subsidence regions acts to balance radiational cooling. Therefore, if one assumes that radiative cooling is the sole diabatic influence on the area surrounding the cluster, a compensating subsidence may be calculated. Following Haltiner and Martin (1957), the radiatively induced subsidence (ω_R) may be expressed as:

$$\omega_R = \frac{-g}{c_p} \frac{\partial \bar{F}_n}{\partial p} \left[\frac{P}{1000}^{R/c_p} \frac{\partial \bar{\theta}}{\partial p}\right]^{-1} . \qquad (5)$$

Where F_n is the net radiative energy flux in Wm^{-2}, g is gravitational acceleration. C_p is specific heat at constant pressure and θ represents potential temperature. Based on the above assumptions, and allowing for no horizontal temperature advection, ω_R may be set equal to $\bar{\omega}_{down}$. A mean radiative convergence profile $(\partial \bar{F}/\partial p)$, is obtained by averaging each of the Cox/Griffith box values for radiative

convergence which fall outside of the cloud cluster area. Ship sounding data from the subsidence region are averaged to obtain $\partial\overline{\theta}/\partial p$. The result is a vertical profile of ω_{down}, calculated for nine 100 mb layers in the troposphere.

Rearranging Eq. (4), the mean vertical profile of the cloud cluster region may be calculated as follows:

$$\overline{\omega}_{up} = \frac{\overline{\omega}_{A/B}\ A_{A/B} - \overline{\omega}_{down}\ A_{down}}{A_{up}} \tag{6}$$

where the calculation is carried out layer by layer to preserve the mass balance.

This $\overline{\omega}_{up}$ profile represents the net upward motion within the cloudy region. This is not to say that there is upward motion everywhere within the cluster area. Indeed, Johnson (1980) diagnosed that convective and mesoscale downdrafts occurring within the cluster region are significant factors in the overall heat, mass and water budgets of a composite tropical wave system. An idealized depiction of this $\overline{\omega}$ model for the A/B array appears in Figure 15.

Larger scale radiative effects are assessed by defining some large scale horizontal area (A_{TOT}) in which there is assumed to be no mass flux across the boundaries. In this area, the total mass transport upward within the cloud cluster ($\overline{\omega}_{up}\ A_{up}$) is equal to the total mass descending ($\overline{\omega}_{down}\ A_{down}$), i.e. ($\overline{\omega}_{TOT} = 0$) in the surrounding environment such that:

$$\overline{\omega}_{TOT}\ A_{TOT} = 0 = \overline{\omega}_{up}\ A_{up} + \overline{\omega}_{down}\ A_{down}. \tag{7}$$

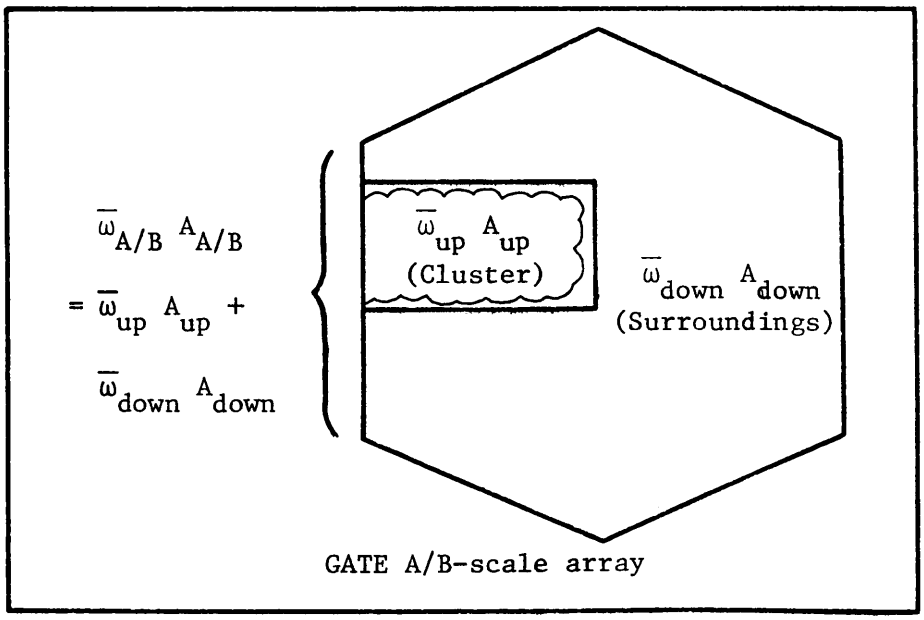

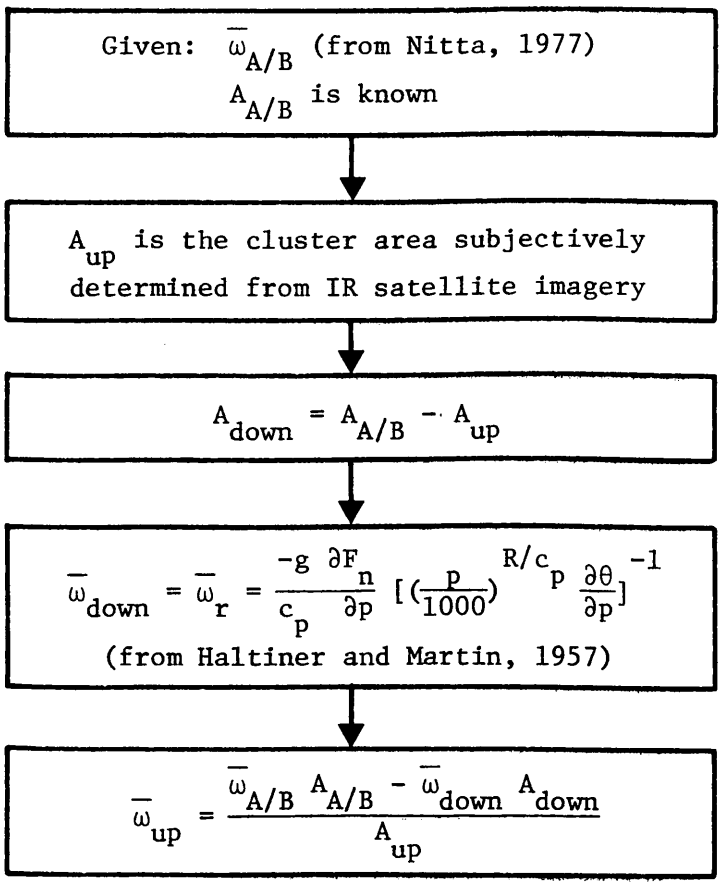

Figure 15. Conceptualization of the radiatively derived A/B-scale vertical motion model.

A mean vertical motion value for the tropospheric column is obtained for the ascending and descending regions from the respective vertical $\overline{\omega}$ profiles. The $\overline{\omega}_{up}$, A_{up} and $\overline{\omega}_{down}$ values are the same as calculated for the A/B array. This, of course, assumes that the radiative characteristics of the cluster and surrounding regions located outside of the A/B array approximates those of their respective regions within the array. The value for A_{down} is left to be solved for by:

$$A_{down} = \frac{\overline{\omega}_{up} A_{up}}{\overline{\omega}_{down}} \tag{8}$$

and,

$$A_{TOT} = A_{up} + A_{down}.$$

This A_{TOT} represents the total "area of influence" of the cloud cluster, when only radiative effects are considered in the subsidence calculation. For budget calculations, Gray (1979b) has introduced the so-called "sphere of influence" for a cloud cluster. This is based on a closed system where total mass transport upward in the cloud cluster is equal to the mass transport downward over a much larger area of weaker subsidence surrounding the cluster. The corresponding mean vertical motion of this idealized system is therefore zero. Hence the sum total of the cloud cluster area and the adjacent subsidence region may be considered the "total area" (A_{TOT}) of the system. The A_{TOT} of a cloud cluster may be qualitatively inferred from examination of satellite imagery for suppressed regions between disturbance areas.

The A_{TOT} calculated for the present study is unique in that the A_{down} and $\bar{\omega}_{down}$ values are derived primarily from radiative considerations. This may not be altogether realistic in light of other dynamic factors involved; however, examination of the satellite imagery with regard to A_{TOT} yields some interesting results which shall be covered in the next section. The area used for the satellite determination is derived by incrementing outward in all directions a distance ΔX from the satellite determined cluster boundaries, so that the calculated radiative A_{TOT} is satisfied. An idealized depiction of the total area concept just discussed appears in Figure 16.

4.3.2 Results

The cloud cluster area (A_{up}) was defined from the satellite as a box encompassing 8-11°N and 18-25.5°W for the 0600-1200 LST case and 6-10°N and 22-30°W for the 1800-2400 LST case. The cluster area covered 46% of the 177 box A/B array for the 0600-1200 LST (daytime) period and 54% of the A/B array for the 1800-2400 LST (nighttime) period.

The vertical motion regimes of the daytime and nighttime cases appear in Table 2. It should be noted that the cluster was approaching its mature stage in the daytime period, while rapid dissipation was occurring during the nighttime period. As a result, the magnitude of $\bar{\omega}_{A/B}$ from Nitta (1977) is considerably smaller in the 1800-2400 LST case. The mean tropospheric $\bar{\omega}_{down}$ value is roughly three times greater for the nighttime case (+ 1.37 mb/hr^{-1}) than for the daytime case (+ 0.43 mb/hr^{-1}). This is expected when one considers the much larger cooling rates at night when there is an absence of SW heating

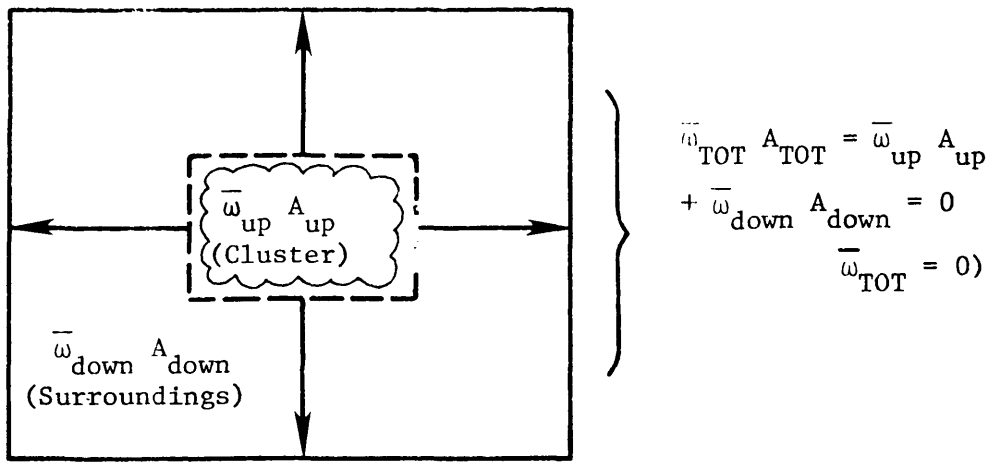

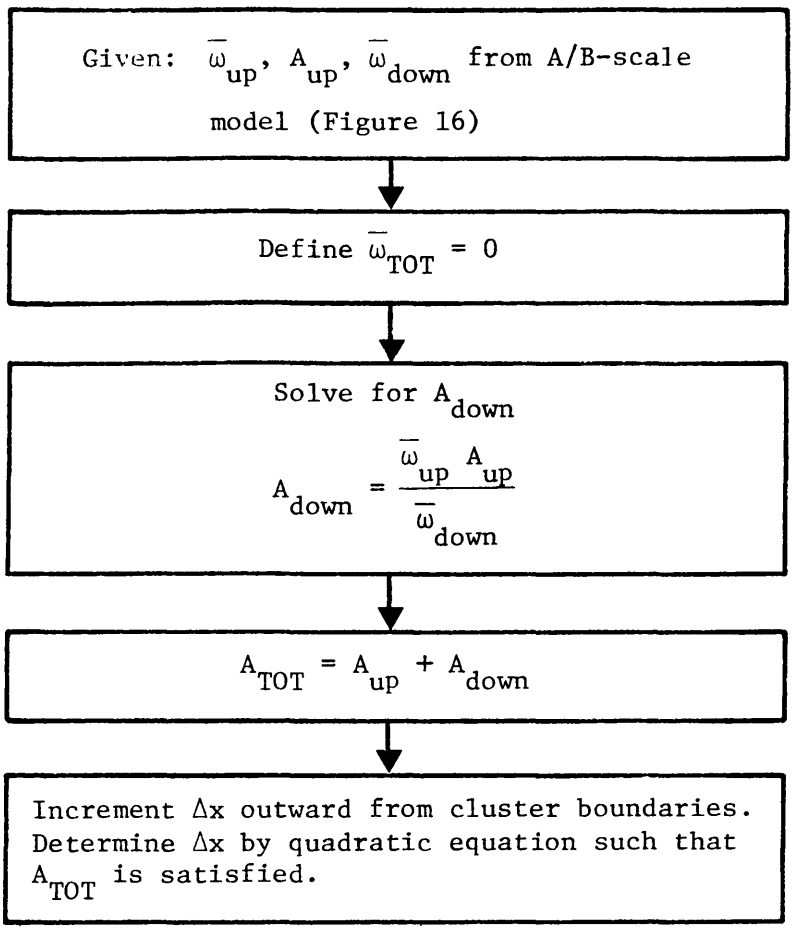

Figure 16. Conceptualization of the radiatively derived total area (A_{TOT}).

MODEL VERTICAL MOTION PROFILES

LAYER (mb)	$\overline{\omega}_{A/B}$ 06-12	$\overline{\omega}_{A/B}$ 18-24	$\overline{\omega}_{down}$ 06-12	$\overline{\omega}_{down}$ 18-24	$\overline{\omega}_{up}$ 06-12	$\overline{\omega}_{up}$ 18-24
100-200	-1.0	0.0	0.003	0.1	-2.2	-0.1
200-300	-5.0	-3.0	0.3	1.2	-11.1	-6.4
300-400	-7.5	-4.0	0.2	2.2	-16.4	-9.1
400-500	-7.0	-4.0	0.2	1.6	-15.3	-8.6
500-600	-7.5	-4.5	0.5	1.9	-16.7	-9.8
600-700	-8.0	-5.0	0.7	1.9	-18.0	-10.7
700-800	-8.0	-5.0	0.8	1.4	-18.1	-10.3
800-900	-7.0	-5.0	0.6	1.0	-15.7	-10.0
900-1000	-3.0	-2.0	0.5	1.0	-6.9	-4.5
MEAN	-6.0	-3.6	0.4	1.4	-13.4	-7.7
mb/day^{-1}	-144.0	-86.7	10.3	33.0	-321.3	-185.3

Table 2. Profiles of various components of vertical p-velocity within the GATE A/B-scale array for 0600-1200 LST and 1800-2400 LST on 5 September 1974.

influences. Despite the larger $\bar{\omega}_{down}$ values during the nighttime period, the mean tropospheric cluster area vertical motion of -7.72 mb/hr^{-1} is substantially smaller than the -13.39 mb/hr^{-1} for the daytime case. Both $\bar{\omega}_{up}$ profiles show a broad layer of fairly constant maximum vertical motion from 800 mb up to the 300 mb level. The vertical motion maximum does not seem to be migrating to lower tropospheric levels during the nighttime dissipation period, however.

A question arises as to just how much of the diurnal variation in radiative forcing is due to the SW heating cycle and how much might be attributable to variations in cloudiness. Figure 17 shows the vertical profile of mean cloud top distribution for the day and night cases and the associated mean LW convergence values in the area surrounding the cloud cluster. It is readily apparent that there are many more middle tropospheric clouds in the nighttime case, and more low cloudiness in the morning case. The corresponding LW convergence profiles for the two periods show larger negative convergence values in the 300-600 mb layer from the higher cloud top amounts present in that region during the nighttime case. Below 600 mb, the larger clear sky percentage in conjunction with a larger amount of low cloud tops result in greater negative convergence values in the daytime case. Despite the discrepancies mentioned, the total tropospheric LW convergences for the two cases are quite similar; 199.85 Wm^{-2} $(912\ mb)^{-1}$ for the daytime case and 195.01 Wm^{-2} $(912\ mb)^{-1}$ for the nighttime case. For the cluster surroundings, it appears that the daytime SW heating superimposed upon LW cooling is the overwhelming factor accounting for the diurnal radiative convergence differences. This statement applies to

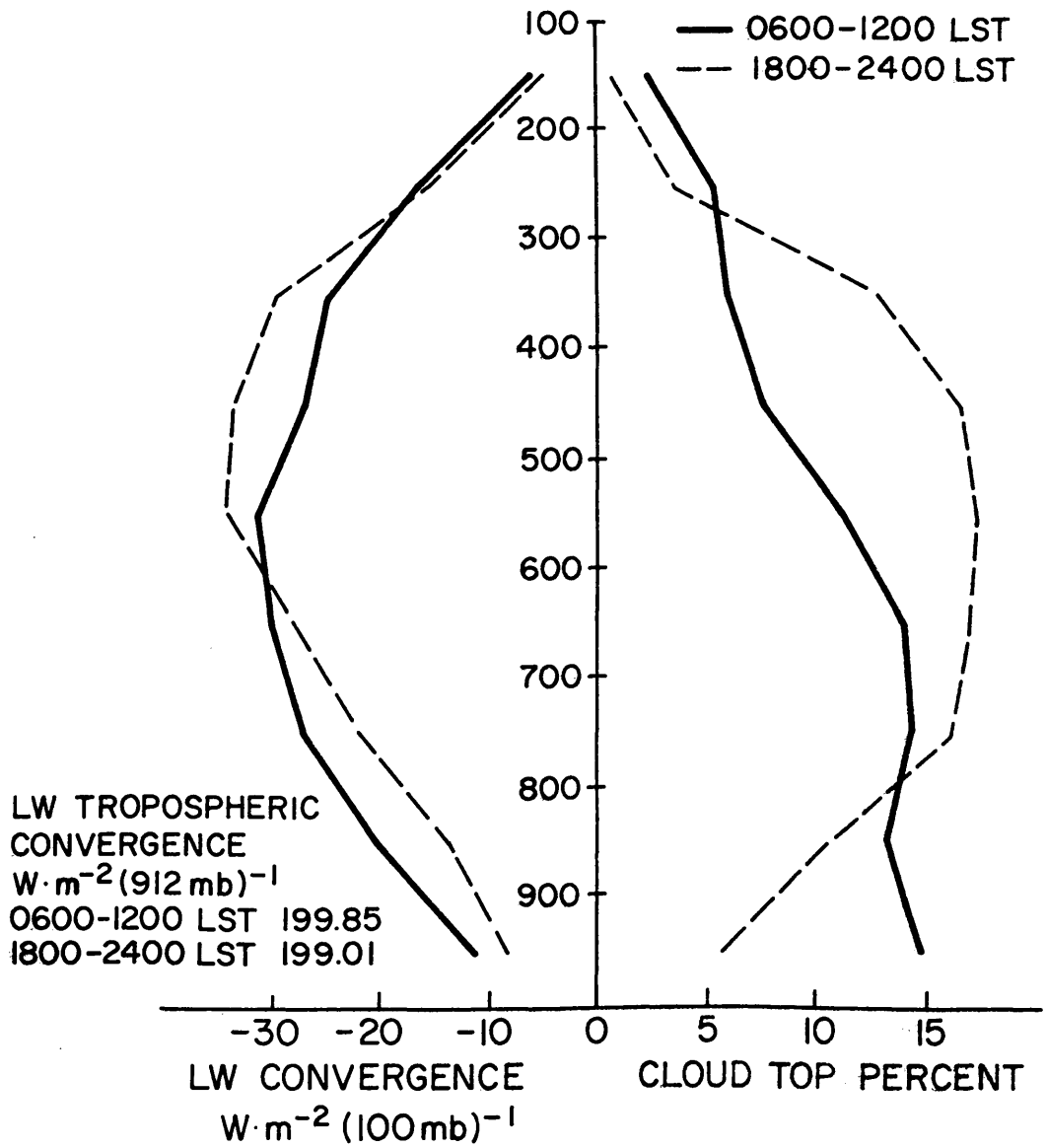

Figure 17. LW convergence and cloud top distribution for the regions surrounding the cluster for 0600-1200 LST (dashed) and 1800-2400 LST (solid) on 5 September 1974.

the troposphere as a whole, although cloudiness variations do have effects on individual layers.

Consider now the results of the aforementioned radiative "sphere of influence" calculation. Extending the subsidence area outward to a point where downward and upward mass transport within the system are equal, "total area" (A_{TOT}) was calculated for both periods. The daytime calculation yields an A_{down} some 31.2 times larger than the cluster area, A_{up}. This is reasonable, in light of the high upward mass transport within the cluster area, and the comparatively small downward mass transport per unit area of the surrounding region encountered in the daytime case. In contrast, the nighttime period yielded an A_{down} that is some 5.6 times larger than the observed cluster area. This was a consequence of larger nighttime mass transport downward due to LW cooling coupled with smaller upward mass transport within the dissipating cluster.

Next, the satellite imagery is examined in Figures 18 and 19. The total area (A_{up} and A_{down}) encompasses a box 4°S - 23°N and 6° - 37.5°W for the 0600-1200 LST case; and 1.5° - 14.5°N, 17.5° - 34.5°W for the 1800-2400 LST case. Ignoring the convective activity over and immediately adjacent to the African continent, the most notable convective feature is an apparent cluster system centered at 14°N, 41.5°W in the 1030 GMT (0900 LST) imagery. By 2230 GMT (2100 LST) it appears to have intensified somewhat, while migrating westward to a point 13.5°N, 45°W. For the morning case, the radiatively derived total area extends westward $\sim$ 80% of the way to this second cloud cluster. Even accepting the fact that the second cluster appears less intense, the total area of the GATE cluster seems too large, overlapping the area

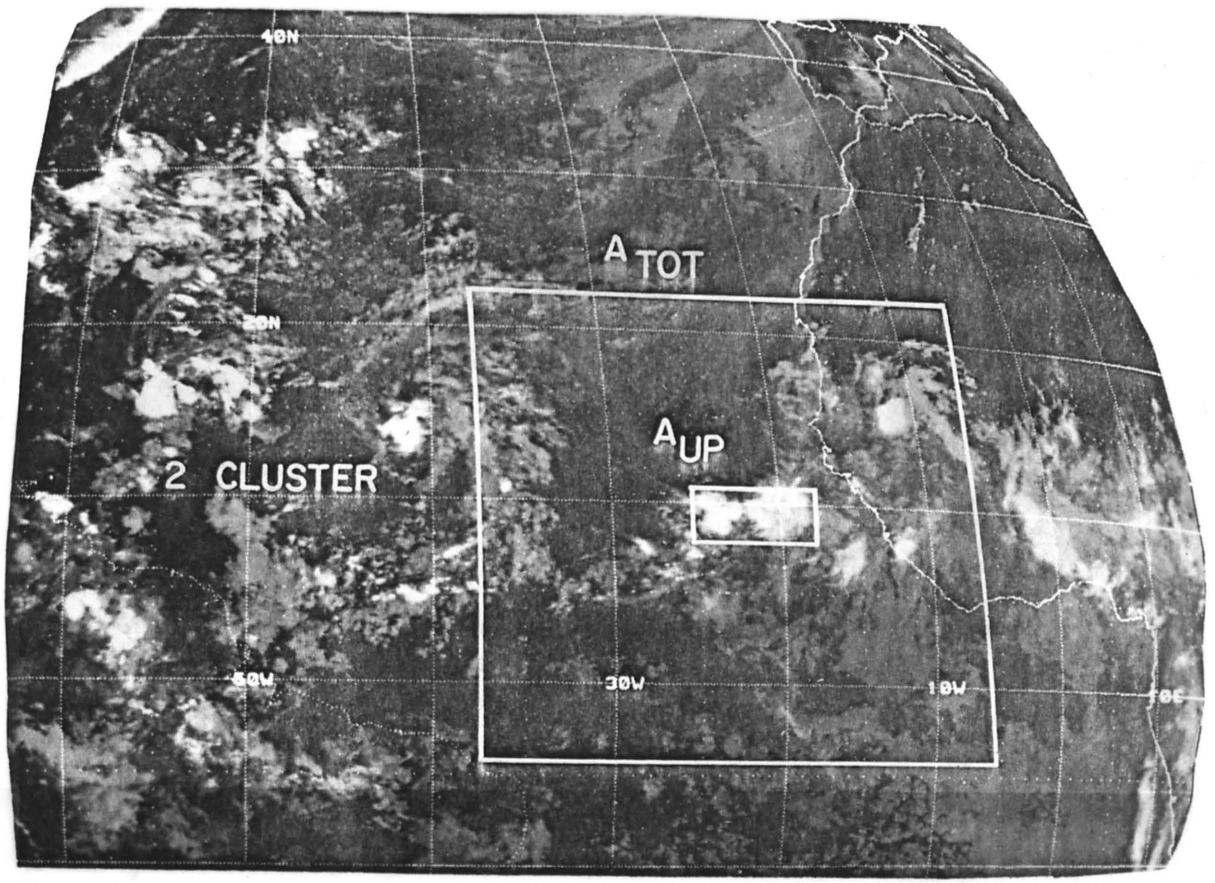

Figure 18. Graphical depiction of the GATE cluster area (A_{up}) and the total area (A_{TOT}) for 0600-1200 LST on 5 September. The infrared satellite imagery is for 0900 LST (1030 GMT).

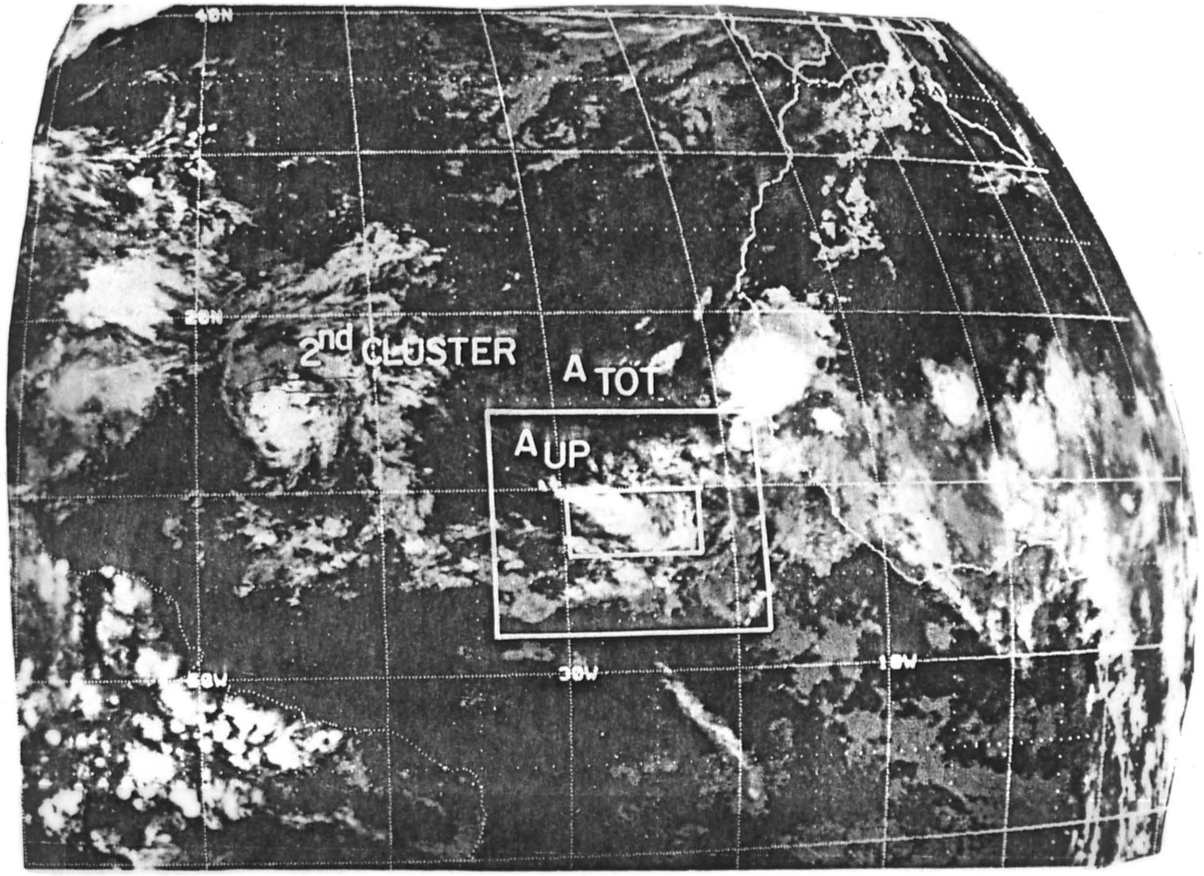

Figure 19. Graphical depiction of the GATE cluster area (A_{up}) and the total area (A_{TOT}) for 1800-2400 LST on 5 September. The infrared satellite imagery is for 2100 LST (2230 GMT).

of the second cluster. Examination of the nighttime imagery reveals that the total area extends roughly one-half a wavelength westward toward the second cluster. During this nighttime period, the two clusters seem much more comparable as far as convective activity is concerned. Assuming, therefore, that the total areas of the clusters are comparable, the nighttime radiationally derived total area seems to be a much more realistic representation of the actual total area. It should be emphasized that this is a very qualitative assessment of radiative influences for a single case study, and is not necessarily representative of other cluster regimes.

4.3.3 Model Sensitivity

Figure 20a-b shows the overall effect of imposing certain errors upon the calculated $\bar{\omega}_{up}$ values within the cluster. Profile A of each graph shows the calculated $\bar{\omega}_{up}$ profiles for the two cases discussed in the preceding paragraphs. Profile B assumes the $\bar{\omega}_{down}$ due to radiation is zero, testing the sensitivity of the $\bar{\omega}_{up}$ calculation to radiative convergence values. It is readily apparent that the $\bar{\omega}_{up}$ profile of the morning case is relatively insensitive to errors in the small radiative convergence values during that period. There is only a 3% difference in the mean tropospheric $\bar{\omega}_{up}$ for the 0730-1330 GMT case. The elimination of compensating subsidence during the nighttime case reveals somewhat greater sensitivity due to the neglect of large nighttime LW radiational cooling. Imposing this unrealistically large error, reduces the tropospheric $\bar{\omega}_{up}$ profile by only 15%.

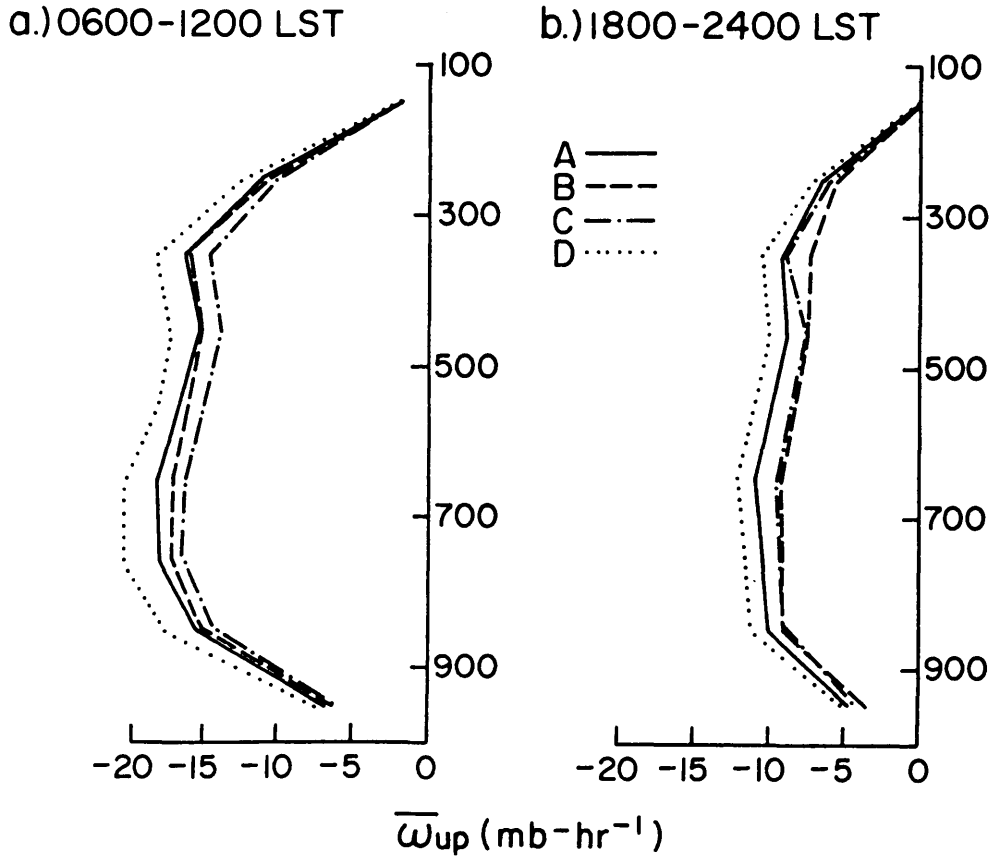

Figure 20. Sensitivity of the $\overline{\omega}_{up}$ profile to various imposed errors. A represents the model value for $\overline{\omega}_{up}$; B represents the assumption that $\overline{\omega}_{down} = 0$; C represents a 10% overestimation of cluster area; D represents a 10% underestimation of cluster area.

Even though the $\bar{\omega}_{up}$ profiles seem relatively insensitive even to abnormally large errors in radiative convergence, they must be tested further for sensitivity to errors in cluster area determination. The final two profiles (C and D) in Figure 20 represent the calculated $\bar{\omega}_{up}$ profiles for 10% overestimation and 10% underestimation of cluster area determination, respectively. For a 10% overestimation in A_{up}, the mean tropospheric $\bar{\omega}_{up}$ value was reduced by 9% for the daytime case and 10% for the nighttime case. The $\bar{\omega}_{up}$ values were slightly more sensitive for the 10% underestimation in cluster area, yielding 12% and 13% increases for the daytime and nighttime cases respectively. Despite the large imposed errors, the observed sensitivity of the $\bar{\omega}_{up}$ profile is well within the instrumental and interpolation errors of the $\bar{\omega}_{A/B}$ determination from which the original $\bar{\omega}_{up}$ profile was derived.

V. IMPLICATIONS

The previous chapters have yielded results which show significant variations in radiative forcing on the diurnal, as well as cluster lifetime scale. Therefore, it is necessary to evaluate these results and explore the possible roles radiative forcing may play on dynamical interactions between the cluster and the large scale environment. It should be emphasized that it is rather difficult to make general inferences on the basis of a case study of an individual cloud cluster. Thus, the implications set forth here are based upon this single cloud cluster, with the full realization that other cloud clusters in various large scale regimes may exhibit inherently different characteristics.

The "slab" and cross section analyses have revealed a distinct evolution of the radiative convergence field during the life cycle of the cloud cluster. The strongest horizontal radiative convergence gradients are observed to occur in the initial nighttime periods from 1800 LST 4 September - 0600 LST 5 September. Although much of the radiative forcing appears to be collocated with the dying squall line system during the first six hour period, a noticeable expansion of the area of forcing occurs during the following six hours. According to Leary and Houze (1979), the cluster is in its initial and developing stages during this period. Therefore, strong gradients of horizontal radiational cooling may play an important role in the establishment of an enhanced inflow regime at low levels and an increased outflow regime at upper levels during the initial stages of cluster development. The

inflow-outflow regime is comparable to that set forth by Gray and Jacobson (1977).

As SW warming is superimposed upon LW cooling, the gradients weaken considerably during the daytime 0600-1800 LST period. Despite this, the system continues to intensify, with a peak in activity occurring in the early afternoon hours. Figure 21 shows the hourly rainfall rates for the GATE master radar array, which covers most of the B-array, and the TTC forcing from Table 2. Although the B-array constitutes a rather small section of the overall analysis area, the radar covers 25-40% of the convective area during each time period. It appears that this is a large enough coverage area to qualitatively mirror cloud cluster intensity, as the array precipitation values are in reasonable temporal agreement with intensity variations discussed by Leary and House (1979).

Figure 21 clearly shows that the peak in cluster precipitation intensity occurs at about 1330 LST, some seven to eight hours after the termination of strong nighttime radiative forcing just after sunrise. If an analogy is drawn between array-averaged precipitation intensity and instances of heavy rainfall, comparison of results to those of Gray and Jacobson (1977) may be made.

The observed maximum in cluster precipitation intensity is in general agreement with the findings of Gray and Jacobson (1977), which show an afternoon maximum in heavy precipitation over the GATE region. However, the cluster precipitation maximum does occur several hours later than the mid morning maximum observed over other oceanic regions. Gray and Jacobson attribute the anomalous GATE maximum to large low level wind shear and instances of squall line activity initiated in

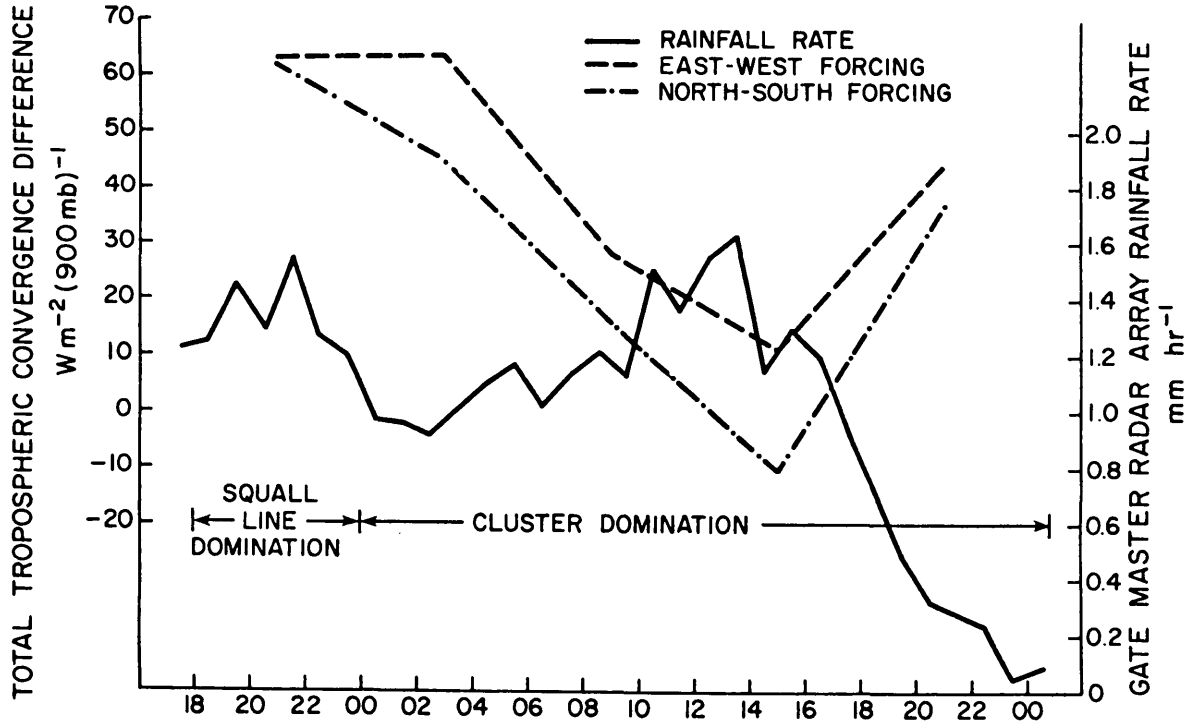

Figure 21. GATE master radar array rainfall rate (——) and the mean zonal (---) and meridional (-.) radiative forcing from Table 1. The arrows delineate time periods when precipitation was dominated by the squall line rathern than the cluster system.

part by African continental influences. It appears, then, that forcing from continental-oceanic and Hadley circulation regimes is exerting a significant influence upon the dynamics of the cluster.

As the cluster system begins to slowly dissipate, the radiative forcing becomes increasingly disorganized. Despite the already weak nature of the daytime radiative convergence gradients, a further gradient relaxation and even a reversal occurs at middle levels between the 0600-1200 LST and the 1200-1800 LST case. The gradients strengthen noticeably in the absence of SW heating in the 1800-2400 LST period; however, they continue to be considerably weaker and less organized than in the initial nighttime case. The reason for the increased disorganization of radiative cooling gradients as the system matures and dissipates is twofold. First, cirrus clouds tend to dissipate or be advected eastward in the strong flow regime at upper levels. As a result, the cluster area loses some of its horizontal uniformity in radiative cooling and the system boundaries become less well defined. This leads to a breakdown of concentrated horizontal gradients of radiative convergence in the cluster boundary regions at upper levels. The second reason involves significant amounts of scattered to broken middle level cloudiness which represent remnants of previous convection. The presence of these clouds brings about the same effects in the middle level radiative convergence fields as observed at cirrus levels. From a radiative standpoint, the maturing of this cluster produces features which ultimately lead to a breakdown of organized radiative forcing upon the system.

A very important feature was noted in the meridional (N-S) and zonal (E-W) cross sections. These cross sections indicate that, for a

localized region, E-W forcing is of comparable magnitude to N-S forcing. However, the N-S forcing for this particular system must be considered more significant, due to the E-W elongation of the system. Nevertheless, this observation is in agreement with the modeling results of Stephens and Webster (1979) and Albrecht and Cox (1975), which show that longitudinal radiative forcing is significant and may modulate convective disturbances. The results of those studies and the present one indicate a need to account for longitudinal as well as latitudinal gradients of radiative cooling in order to more adequately model atmospheric circulation characteristics.

The simple ω model, which was constructed in order to assess the overall role of radiation in the dynamical interactions of the cloud cluster with the large scale environment, yielded some interesting results. The calculation of surrounding area downward vertical motion by a purely radiative means may admittedly be an oversimplification. Nevertheless, for p>300 mb, the nighttime $\bar{\omega}_{down}$ profile derived by purely radiative means exhibits qualitative similarites to an environmental subsidence profile diagnosed by Johnson (1980) for the trough region of a composite tropical wave.

Perhaps more interesting is the cluster raditive "total area of influence" calculation performed with the same radiation simplification. Although the computed total area appeared to be unrealistically large for the weak forcing of the daytime calculation, the nighttime radiative total area appeared qualitatively similar to the area one might independently derive through interpretation of satellite imagery. Although the calculations are rather rough, there is the suggestion that, during the nighttime, when radiative forcing is strongest,

radiation may play a significant role in the cluster-scale dynamical interaction with the surrounding environment. The daytime values are weakened to the point that they are probably, at best, a secondary influence, with continental-land interactions due to daytime heating differences dominating the system dynamics.

The unrealistically large radiatively derived total area for the daytime case may be predominantly due to the model assumption of a closed mass system. Admittedly, this is an oversimplifying assumption. Realistically allowing for net mass flux across area boundaries would effect a change in the size of the total area necessary to achieve a mass balance. For instance, allowing for mass divergence outward across area boundaries would necessarily bring about a smaller resultant total area, if all other parameters are held constant. The unrealistically large total area suggests that significant mass flow across area boundaries is occurring in the daytime case, rendering the closed system assumption suspect. Apparently there is significant cluster scale interaction with the large scale circulation pattern during the daytime period. The interactions appear to be somewhat more localized in the nighttime case, suggesting that little mass flow occurs across area boundaries. The result is a realistic total area calculation based on the closed system and radiative assumptions for the nighttime case. It should be emphasized that the calculated values presented herein are merely two individual cases in the lifetime of one of a myriad of convective disturbances occurring throughout the global system.

The implications presented in this chapter are ones which, at best, are only applicable to this cloud cluster regime. While study

of further individual case studies is beyond the scope of this report, there does exist a need for similar case studies from which a much more complete understanding of the role of radiation in cluster dynamics may be derived.

VI. CONCLUSIONS

"Slab" analyses and horizontal cross section analyses of radiative convergence fields have yielded a three dimensional representation of radiative forcing upon the cloud cluster contained within the GATE A/B array from 4-6 September 1974. Horizontal gradients of radiative convergence are largest in the middle levels and progressively weaker at lower and higher levels, respectively. This forcing is strongest during the period from 1800-0600 LST 4-5 September 1974 in the initial stages of the cluster life cycle. As the daytime SW warming is superimposed upon the LW cooling (0600-1800 LST), the gradients in radiative convergence weaken considerably relative to the initial nighttime period. During the 1200-1800 LST period, the already weakened gradients become even more diffuse, with a reversal in horizontal radiative forcing at lower and middle levels in some regions. Although the forcing does intensify during the 1800-2400 LST period, it is substantially weaker and less concentrated than in previous nighttime periods. Throughout the cluster lifetime, E-W radiative forcing is comparable to N-S forcing over localized regions.

A simple model of vertical motion has been constructed to investigate potential effects of radiative forcing on cluster-scale dynamical interaction with the large scale atmospheric circulation. The downward vertical motion calculation in regions surrounding the cluster has been simplified to include radiative cooling as the sole component of diabatic heating. Cluster and surrounding vertical motions have been calculated for a daytime (0600-1200 LST) and a nighttime (1800-2400 LST) period of 5 September.

The radiatively derived subsidence profile was qualitatively similar to the environmental subsidence profile in the trough region of a tropical wave composite diagnosed by Johnson (1980). Total areas of influence, whereby upward mass transport within the cloud cluster area equals downward mass transport in surrounding areas, have been determined for the two cases. Examination of satellite imagery has revealed that the radiatively derived total area of the daytime case was much too large to be deemed realistic. However, the radiatively derived total area of the nighttime case seems a qualitatively reasonable representation of the actual total area of influence, extending roughly one-half the distance to an adjacent cluster possessing qualitatively similar characteristics.

On the basis of these analyses several suggestions may be made about the role of radiative forcing on this cloud cluster system. Radiative forcing was strongest during the initial stages of cluster development. Suppressed nighttime LW cooling in the low and middle levels of the disturbance region relative to the surrounding environment leads to a lowering of cluster pressure and a subsequent increased inflow into the cluster region. At higher levels above 300 mb, greater relative LW cooling at disturbance cloud top levels results in an increased outflow from the disturbance due to radiatively induced pressure differences.

As the system intensified, two major factors led to the weakening and decreased organization of horizontal gradients of radiative convergence between the cluster and its surrounding environment. The first was the substantial reduction of radiative forcing due to SW warming superimposed upon LW cooling. Increased amounts of surrounding area

middle and high cloud remnants, formerly associated with active convection, contribute to less concentrated and more poorly organized gradients of radiative convergence.

The E-W gradients were found to be comparable in magnitude to the N-S gradients over localized regions. Although the overall N-S forcing was greater due to the E-W elongation of the disturbance, the results suggest that the longitudinal gradients in radiative cooling are significant. Albrecht and Cox (1975) and Stephens and Webster (1979) present further evidence which indicates that longitudinal variations in radiative convergence need to be addressed in order to more adequately model general circulation patterns.

The 6-8 hour lag of the most intense precipitation behind the incidence of strong radiative forcing is in general agreement with GATE composite observations. However, the time of maximum precipitation occurs several hours later than the mid morning maximum observed in mid oceanic regions. Since the analysis area is relatively close to the African continent, circulation modulated by continental-oceanic differential heating is likely to have a significant role in modulating the cluster dynamical interactions with the large scale environment.

The radiatively based vertical motion calculation yielded a qualitatively realistic total area of cluster influence for the nighttime 1800-2400 LST period. This result suggests that radiative forcing may have a significant influence upon cluster interaction with the surrounding subsident region during the night, when radiative forcing is strongest. The model assumption of a closed mass system appears to break down during the daytime period. This suggests a significant

cluster scale interaction with the larger scale circulation of a much greater magnitude than could be explained by purely radiative means.

It is quite difficult to make generalizations about radiative forcing upon cluster disturbances solely on the basis of an individual case study. Therefore, more studies of this type are needed if the role of radiative forcing upon cloud cluster and large scale dynamical interaction is to be fully appreciated.

REFERENCES

Ackerman, S. A., and Stephen K. Cox, 1980: GATE Phase III mean synoptic scale radiative convergence profiles. Dept. Atmos. Sci. Paper 324, Colorado State University, Fort Collins, CO., 119 pp.

Albrecht, B. A., and Stephen K. Cox, 1975: The large scale response of the tropical atmosphere to cloud modulated infrared heating. J. Atmos. Sci., 32, 16-24.

Arkell, R., and Michael Hudlow, 1977: GATE International Meteorological Radar Atlas. National Oceanic and Atmospheric Administration, Environmental Data Service, 222 pp.

Cox, S. K., 1973: Infrared heating calculations with a water vapour pressure broadened continuum. Quart. J. Roy. Meteor. Soc., 99, 669-679.

_____, M. Polifka, K. Griffith, T. Rockwood and D. Starr, 1976: Radiative transfer computational routines for atmospheric science applications. Colorado State University Atmospheric Science Research Report, 75 pp.

_____, and K. T. Griffith, 1978: Tropospheric radiative divergence during Phase III of the GARP Atlantic Tropical Experiment (GATE). Dept. Atmos. Sci. Paper 291, Colorado State University, Fort Collins, CO., 166 pp. [NTIS PB292761]

_____, and K. T. Griffith, 1979a: Estimates of radiative divergence during Phase III of the GARP Atlantic Tropical Experiment, Part I. Methodology. J. Atmos. Sci., 36, 576-585.

_____, and K. T. Griffith, 1979b: Estimates of radiative divergence during Phase III of the GARP Atlantic Tropical Experiment, Part II. Analysis of Phase III results. J. Atmos. Sci., 36, 586-601.

Dopplick, T. G., 1972: Radiative heating of the global atmosphere. J. Atmos. Sci., 29, 1278-1294.

Foltz, G. S., 1976: Diurnal variation of the tropospheric energy budget. Dept. Atmos. Sci. Paper 262, Colorado State University, Fort Collins, CO., 140 pp.

Gray, W. M., and R. W. Jacobson Jr., 1977: Diurnal variation of deep cumulus convection. Mon. Wea. Rev., 105, 1171-1188.

_____, 1979a: Hurricanes/their formation, structure and likely role in the tropical circulation. Quart. J. Roy. Meteor. Soc., 105, 155-218.

_____, 1979b: Personal Communication.

REFERENCES (Continued)

Haltiner, G. S., and F. L. Martin, 1957: Dynamical and physical meteorology. McGraw-Hill Book Company, Inc.

Houze, R. A. Jr., 1977: Structure and dynamics of a tropical squall-line system. Mon. Wea. Rev., 105, 1540-1567.

Hudlow, M. D., and V. L. Patterson, 1979: GATE Radar Rainfall Atlas. National Oceanic and Atmospheric Administration, Environmental Data and Information Service, 155 pp.

Johnson, R. M., 1980: Diagnosis of convective and mesoscale motions during Phase III of GATE. J. Atmos. Sci., 37, 733-753.

Katayama, A., 1966: On the radiation budget of the troposphere over the Northern Hemisphere (I). J. Meteor. Soc. Japan, 44, 381-401.

_____, 1967a: On the radiation budget of the troposphere over the Northern Hemisphere (II). J. Meteor. Soc. Japan, 45, 1-25.

_____, 1967b: On the radiation budget of the troposphere over the Northern Hemisphere (III). J. Meteor. Soc. Japan, 45, 26-39.

Leary, G. A., 1979: Behavior of the wind field in the vicinity of a cloud cluster in the Intertropical Convergence Zone. J. Atmos. Sci., 36, 631-639.

_____, and Robert A. Houze Jr., 1979a: The structure and evolution of convection in a tropical cloud cluster. J. Atmos. Sci., 36, 437-457.

_____, and Robert A. Houze Jr., 1979b: Melting and evaporation of hydrometeors in precipitation from the anvil clouds of deep tropical convection. J. Atmos. Sci., 36, 669-679.

Nitta, T., 1977: Response of cumulus updraft and downdraft to GATE A/B scale motion system. Tropical Meteorology Paper 18, Dept. Atmos. Sci., U.C.L.A., Los Angeles, CA., 46 pp.

Polifka, M. Charlene, and Stephen K. Cox, 1977: GATE SMS-1 brightness frequency distribution digital magnetic data tapes. Dept. Atmos. Sci. Research Report, Colorado State University, Fort Collins, CO., 25 pp.

Smith, E. A., and T. H. Vonder Haar, 1976: Hourly synchronous meteorological Satellite-1 (SMS-1) data collected during the GARP Atlantic Tropical Experiment (GATE). Earth located, edited data set. Dept. Atmos. Sci. Research Report, Colorado State University, 180 pp.

REFERENCES (Continued)

Stephens G. L., and Peter J. Webster, 1979: Sensitivity of radiative forcing to variable cloud and moisture. J. Atmos. Sci., 36, 1542-1556.

Webster, Peter J., and G. L. Stephens, 1980: Tropical upper-tropospheric extended clouds: Inferences from Winter MONEX. J. Atmos. Sci., 37, 1521-1541.

Zaitseva, N. A., 1976: The spatial and temporal variability of long-wave radiation fields of GATE-74. Proceedings of the IAMAP International Radiation Symposium, 19-28 August, Garmisch-Partenkirchen, FRG., p. 530.

_____, and H. P. Fimpel, 1976: Report on the radiometersondes intercomparison during GATE to the Radiation Commission IAMAP. Personal Communication.

BIBLIOGRAPHIC DATA SHEET	1. Report No. CSU-ATS	2.	3. Recipient's Accession No.
4. Title and Subtitle			5. Report Date November, 1980
			6.
7. Author(s) Gregory P. Byrd and Stephen K. Cox			8. Performing Organization Rept. No. CSU-ATS-
9. Performing Organization Name and Address Department of Atmospheric Science Colorado State University Fort Collins, CO 80523			10. Project/Task/Work Unit No. 11. Contract/Grant No. ATM 78-05743
12. Sponsoring Organization Name and Address National Science Foundation, NOAA			13. Type of Report & Period Covered 14.

15. Supplementary Notes

16. Abstracts Tropospheric radiative convergence profiles from Cox and Griffith (1978) are used to assess the radiative forcing upon a tropical cloud cluster located in the vicinity of the GATE A/B-scale array during 4-6 September 1974. "Slab" and cross sectional analyses are carried out in order to present a three dimensional view of the radiative convergence field within the cluster and its surrounding regions. Next, a simple vertical motion profile is constructed to investigate the potential effects of radiative forcing upon cluster scale dynamical interactions with the large scale circulation. The model is tested on a daytime and a nighttime case within the cluster life cycle. The ensuing discussion evaluates the analysis and expands upon the possible roles of radiative forcing upon cluster scale and large scale dynamics.

17. Key Words and Document Analysis. 17a. Descriptors

Tropical Cloud Clusters GATE Tropical Meteorology

17b. Identifiers/Open-Ended Terms

17c. COSATI Field/Group

18. Availability Statement	19. Security Class (This Report) UNCLASSIFIED	21. No. of Pages 70
	20. Security Class (This Page) UNCLASSIFIED	22. Price

FORM NTIS-35 (Rev. 3-72)